**Affinities of Recombinant Norovirus P Dimers for Human Blood Group Antigens**

Ling Han[1], Pavel I. Kitov[1], Elena N. Kitova[1], Ming Tan[2,3], Leyi Wang[2], Ming Xia[2], Xi Jiang[2,3] and John S. Klassen[1]*

[1] *Alberta Glycomics Centre and Department of Chemistry, University of Alberta, Edmonton, Alberta, Canada T6G 2G2*

[2] *Division of Infectious Diseases, Cincinnati Children's Hospital Medical Center and*

[3]*Department of Pediatrics, University of Cincinnati College of Medicine, Cincinnati, OH, USA*

*Corresponding Author's address:

Department of Chemistry

University of Alberta

Edmonton, AB CANADA T6G 2G2

Email: john.klassen@ualberta.ca

Telephone: (780) 492 3501

SUPPLEMENTARY DATA provided:

Suppl_data.pdf contains Figures S1-S5;

docking_A_pdb.rar contains pdb files with energy optimized structures of type A oligosaccharides docked into binding site of NoV VA387 P dimer;

docking_B_pdb.rar contains pdb files with energy optimized structures of type B oligosaccharides docked into binding site of NoV VA387 P dimer;

docking_H_pdb.rar contains pdb files with energy optimized structures of type H oligosaccharides docked into binding site of NoV VA387 P dimer;

docking_Lewis_pdb.rar contains pdb files with energy optimized structures of Lewis type oligosaccharides docked into binding site of NoV VA387 P dimer.

**Abstract**

Noroviruses (NoVs), the major cause of viral acute gastroenteritis, recognize histo-blood group antigens (HBGAs) as receptors or attachment factors. To gain a deeper understanding of the interplay between NoVs and their hosts, the affinities of recombinant P dimers of a GII.4 NoV (VA387) to a library of 41 soluble analogs of the HBGAs, which contain the A, B, H and Lewis epitopes, with variable sizes (2-6 residues) and different types (1-6) were measured using the direct electrospray ionization mass spectrometry (ESI-MS) assay. The results reveal that the P dimers exhibit a broad specificity for the HBGAs and bind to all of the oligosaccharides tested. Overall, the affinities are relatively low, ranging from 400 to 3000 $M^{-1}$, and are influenced by chain type: 3 > 1 ≈ 2 ≈ 4 ≈ 5 ≈ 6 for H antigens; 6 > 1 ≈ 3 ≈ 4 ≈ 5 > 2 for A antigens; 3 > 1 ≈ 4 ≈ 5 ≈ 6 > 2 for B antigens, but not by chain length. The highest affinity ligands are B type 3 (3000 ± 300 $M^{-1}$) and A type 6 (2350 ± 60 $M^{-1}$). While the higher affinity to the type 3 H-antigen was observed previously, preferential binding to the types 6 and 3 antigens with A and B epitopes, respectively, has not been previously reported. A truncated P domain dimer (lacking the C-terminal arginine cluster) exhibits similar binding. The central binding motifs in the HBGAs were identified by molecular docking simulations.

## Introduction

Noroviruses (NoVs), a group of single-stranded, positive-sense RNA viruses in the *Calciviridae* family, are the major viral pathogens responsible for epidemic acute gastroenteritis in both developed and developing countries. Each year, the viruses infect roughly 20 million people (Lindesmith et al. 2003, Tan and Jiang 2007), resulting in approximately 200 000 deaths (Patel et al. 2008). Currently, there is no effective vaccine or antiviral against NoV infections. Human NoVs can be divided into 2 major genogroups (GI and GII), which contain at least 25 different genotypes (GI.1-8 and GII.1-17) (Tan and Jiang 2005a). The GII.4 is the predominant genotype worldwide causing ~80% of NoV gastroenteritis outbreaks (Tan and Jiang 2007, Yang et al. 2010, Baert et al. 2011, Cannon et al. 2009, Johnston et al. 2007).

The absence of an *in vitro* cell culture system or a suitable animal model has hindered the characterization of NoVs. Consequently, efforts have focused on the recombinant virus-like particles (VLPs). In vitro expression of NoV VP1, the major capsid protein, through recombinant baculoviruses results in the spontaneous assembly of VLPs that are structurally and antigenically indistinguishable from the authentic viruses (Jiang et al. 1992). X-ray crystallography analysis of Norwalk virus VLPs revealed that each of VP1 contains two major domains, the N-terminal shell (S) domain and the C-terminal protrusion (P) domain, linked by a flexible hinge (Prasad et al. 1999). The S domain forms the interior shell of the capsid, while the P domain is responsible for exterior P dimer formation. The P domain exhibits high sequence variability and is important for host-receptor interactions and the host immune response (Tan et al. 2008a, Cao et al. 2007). On its own, the P domain forms homodimers called the P dimers (Tan et al. 2004). The P dimers can

further assemble into larger complexes, a 12-mer small P particle (Tan et al. 2011a) and a 24-mer P particle (Tan and Jiang 2005a, Tan et al. 2008b, Bereszczak et al. 2012). In addition, a soluble P protein in the stool of NoV-infected patients, referred as P polypeptide, has been reported (Hardy et al. 1995, Greenberg et al. 1981) and contains most of the P domain but lacks the highly conserved arginine cluster at the C-terminus and forms a homodimer (Tan et al. 2006, Bu et al. 2008).

NoVs recognize the human histo-blood group antigens (HBGAs) (Huang et al. 2003, Huang et al. 2005, Tan and Jiang 2005b), which play an important role in host susceptibility of NoV. The HBGAs are complex carbohydrates that consist of oligosaccharides covalently linked to proteins or lipids. They are generally present on red blood cells, mucosal epithelia or as free antigens in body fluids, such as blood, saliva, milk and the intestinal contents (Oriol 1990). Although the HBGA phenotype is determined by the terminal part of the oligosaccharide chain linked to protein or lipid, the antigen determinants can be associated with different carbohydrate structures, i.e., precursor chain types. There are six possible types of precursor chains (Oriol 1990). Of these, types 1 - 4 are widely distributed in red blood cells, mucosal epithelia, as well as different organs (Ravn and Dabelsteen 2000), whereas type 6 chain mainly exists in milk and urine (Oriol 1990). The type 5 structure has not been detected in human tissue or secretions. At present, the biological significance of the different HBGA chain types is not fully understood. The carbohydrate moieties of the HBGAs represent the minimum epitope for NoV recognition (Huang et al. 2005, Tan et al. 2008b, de Rougemont et al. 2011, Fiege et al. 2012). NoVs recognize human HBGAs in a strain-specific manner and distinct NoV-HBGA binding patterns

have been described (Huang et al. 2005). The HBGA-binding sites of NoVs are located at the P dimer interface and the recombinant P dimers are shown structurally the same as those of VLP (Cao et al. 2007, Chen et al. 2011, Choi et al. 2008). Thus, the recombinant P dimer and its complex form, the P particle, have been used as models for NoV-HBGA interactions extensively (Tan et al. 2004, Tan and Jiang 2005b, Tan et al. 2006, Tan et al. 2008a, Tan et al. 2008b, Tan et al. 2009, Tan et al. 2011a, Tan et al. 2011b, Tan and Jiang 2012).

At present there are few quantitative data available for the interactions between the NoV VLPs and HBGAs. Peters and coworkers recently investigated such interactions using saturation transfer difference nuclear magnetic resonance (STD-NMR) spectroscopy (Fiege et al. 2012). L-fucose was identified as the minimal structure recognized by a GII.4 VLP (Ast6139) and the association constants ($K_a$) of VLP and the HBGA fragments containing α-L-Fuc are, at best, ~$10^4$ $M^{-1}$. In another study, affinities of $2.6\times10^3$ $M^{-1}$ and $2.2\times10^3$ $M^{-1}$ were measured for a GII.10 P dimer binding to H type 2 trisaccharide and L-fucose, respectively (Hansman et al. 2012).

Here, we describe the first quantitative study of the interactions between GII.4 P dimers, in both their full-length and truncated forms, with HBGA oligosaccharides using the direct electrospray ionization mass spectrometry (ESI-MS) assay (Wang et al. 2003). The affinities of both P dimers for a library of 41 HBGA oligosaccharides, comprising A, B, H and Lewis antigens, were measured at 25 °C and pH 7. In addition, molecular docking simulations were performed to elucidate the structural basis for the trends in the measured affinities.

**Experimental Section**

*Proteins*

Two forms of P dimers of NoV strain VA387 (GII.4) were studied. The first one, referred as P dimer ($P_2$, MW 69,311 Da), was formed from full-length P domain with an amino acid sequence spanning residues 222 to 539 of VA387 VP1 (AAK84679.2). The second one, referred as truncated P dimer (tr-$P_2$, MW 69,006 Da), was formed by a truncated P domain lacking the C-terminal arginine-cluster with a sequence spanning residues 222 to 535 of VA387 VP1 (Tan et al. 2006). Both P dimers were expressed in bacteria through GST-Gene Fusion System (GE-Healthcare Life Sciences) and purified as described previously (Tan et al. 2004, Bu et al. 2008). A single chain fragment (scFv, MW 26,539 Da) of the monoclonal antibody Se155-4, which served as a reference protein ($P_{ref}$) to correct ESI mass spectra for the occurrence of nonspecific ligand binding, was produced using recombinant technology as described elsewhere (Zdanov et al. 1994). Each protein was concentrated and dialyzed against aqueous 50 mM ammonium acetate (pH 7) using Amicon Ultra 0.5 mL centrifugal filters (Millipore Corp., Billerica, MA) with a MW cutoff of 10 kDa and stored at −20 °C until needed. The concentrations of protein stock solutions were measured by UV absorption.

*Carbohydrates*

A complete list of the HBGA oligosaccharides, which range in size from di- to hexasaccharide, is given in Table I; their structures are shown in Figure S1 (Supplementary Data). Compounds **L2**, **L4**-**L6**, **L13**-**L16** and **L24**-**L27** (Meloncelli and Lowary 2009, Meloncelli and Lowary 2010, Meloncelli et al. 2011) were donated by Prof. Todd Lowary (University of Alberta); compound **L23** was donated by Alberta Innovates Technology Futures (Alberta, Canada); compounds **L3**, **L34**, **L36**, **L38** and **L40** were purchased from Dextra (Reading, UK); compounds **L1**, **L6**-**L12**,

**L17**-**L22**, **L28**-**L33**, **L35**, **L37**, **L39** and **L41** were purchased from Elicityl SA (Crolles, France). Two compounds, 3'-siallylactose (**L42**) and 6'-siallylactose (**L43**), which served as negative controls, were purchased from IsoSep AB (Sweden). Stock solutions of each oligosaccharide were prepared by dissolving a known amount of the solid sample in ultrafiltered water (Milli-Q, Millipore) to yield a concentration of 1 mM. The solutions were stored at −20 °C until needed.

*Mass spectrometry*

All of the binding measurements were carried out in positive ion mode using a 9.4T ApexQe Fourier-transform ion cyclotron resonance mass spectrometer (Bruker-Daltonics, Billerica, MA) equipped with a modified nanoflow ESI (nanoESI) source. NanoESI tips were produced from borosilicate capillaries (1.0 mm o.d., 0.68 mm i.d.) pulled to ~5 μm using a P-97 micropipette puller (Sutter Instruments, Novato, CA). A platinum wire was inserted into the nanoESI tip, and a capillary voltage of ~1.0 kV was applied to carry out ESI. Each ESI solution was prepared from stock solutions of P dimer (or truncated P dimer), one of HBGA oligosaccharides and Se155-4 scFv, which served as $P_{ref}$. Aqueous ammonium acetate (10 mM) was added to each solution. In all cases, the P dimer (or truncated P dimer) was incubated with the HBGA oligosaccharide for ~20 min at 25 °C before ESI-MS analysis. For a limited number of HBGA, imidazole (10 mM), which is known to stabilize labile protein-ligand complexes during ESI-MS analysis (Sun et al. 2007, Bagal et al. 2009), was added to the solution to test for the occurrence of in-source (gas-phase) dissociation. Notably, the addition of imidazole did not result in a measurable increase (after correction for nonspecific binding) in the relative abundance of ligand-bound P dimer (Figure S2). These results established that the affinity measurements were

not adversely affected by in-source dissociation. Ions/droplets produced by ESI were introduced into the mass spectrometer through a stainless steel capillary (i.d. 0.43 mm). The capillary entrance and exit voltages were 0 V and 280 V, respectively. The ions were steered by a deflector (250 V) into the first funnel (150 V) and skimmer (20 V) and transmitted through the second funnel (7.5 V) and skimmer (5.0 V), and then accumulated in the first hexapole in-source accumulation cell for 0.6 sec. The ions were then transferred through the quadrupole (using a low m/z cut-off of 1500) followed by further accumulation in a second hexapole collision cell for 0.5 sec. Ions were then transferred to the ICR cell for detection. The pressure in cell region was ~$10^{-10}$ mbar. Data acquisition was performed using the ApexControl software (version 4.0, Bruker-Daltonics, Billerica, MA). The time-domain signal, consisting of the sum of 30 transients containing 32K data points per transient, was subjected to one zero-fill prior to Fourier-transformation.

*Determination of $K_a$ values*

A detailed description of the direct ESI-MS assay can be found elsewhere (Wang et al. 2003, Kitova et al. 2012) and only a brief overview is given here. The assay is based on the detection and quantification of free and ligand-bound protein ions by ESI-MS. The NoV VA387 P dimer possesses two independent and equivalent HBGA binding sites (Cao et al. 2007, Bu et al. 2008). However, as discussed in more detail below, the binding of the HBGA oligosaccharides is very weak ($K_a$ <$10^4$ $M^{-1}$) and only a single bound ligand was observed (after correction for nonspecific binding) under the experimental conditions used. As a result, the reported $K_a$ values correspond to the apparent association constant, which is a factor of two larger than the

microscopic $K_a$.

For a given P dimer-HBGA ligand complex, referred to generally as PL (eq 1), the magnitude of $K_a$ was determined from the ratio ($R$) of total abundance ($Ab$) of ligand-bound (PL) and free protein (P) ions, as measured by ESI-MS for solutions of known initial concentrations of protein ($[P]_0$) and ligand ($[L]_0$), eq 2:

$$P + L \rightleftharpoons PL \tag{1}$$

$$K_a = \frac{R}{[L]_0 - \frac{R}{1+R}[P]_0} \tag{2}$$

where $R$ is calculated using eq 3:

$$R = \frac{Ab(PL)}{Ab(P)} \tag{3}$$

The $K_a$ values reported in Table I correspond to the average value established from replicate (≥3) measurements performed on at least three different HBGA concentrations. In all cases, each ESI mass spectrum was corrected for the occurrence of nonspecific HBGA-protein binding during the ESI process using the reference protein method (Sun et al. 2006). As described elsewhere, this technique involves the addition of a reference protein ($P_{ref}$), which does not bind specifically to the protein and ligand of interest, to the solution. The "true" abundance (in the absence of nonspecific binding) of the ligand-bound and unbound P-dimer is calculated from the measured abundances of ligand-bound and unbound P-dimer. The underlying assumption with the method, that nonspecific ligand binding is a random process and affects equally all proteins in solution regardless of their size or structure, has been rigorously tested and

shown to be generally valid (Sun et al. 2006, Sun et al. 2009, Deng et al. 2010).

For a limited number of oligosaccharides, $K_a$ was determined using a titration approach (Daniel et al. 2002), where the initial concentration of the P dimer was fixed and the concentration of the HBGA ligand was varied. The value of $K_a$ was established from nonlinear regression analysis of the experimentally determined concentration-dependence of the fraction of ligand-bound protein, ($R$/($R$+1)), using eq 4:

$$\frac{R}{R+1} = \frac{1+K_a[\mathrm{L}]_0 + K_a[\mathrm{P}]_0 - \sqrt{(1-K_a[\mathrm{L}]_0 + K_a[\mathrm{P}]_0)^2 + 4K_a[\mathrm{L}]_0}}{2K_a[\mathrm{P}]_0} \quad (4)$$

*Docking simulations*

Molecular models of the interactions between the HBGA oligosaccharides and the P dimer were obtained through a combination of molecular docking and molecular dynamics (MD) simulations. Autodock Vina (Trott and Olson 2010) was used to dock the disaccharide and trisaccharide ligands. Binding modes for the larger HBGA were reconstructed from poses found for smaller, related, HBGA. The crystal structure of the P domain of VA387 bound to the B trisaccharide ligand (**L23**) was used as model of the P dimer binding site (pdb entry: 2obt) (Cao et al. 2007). Protons were added to all heteroatoms using MGL Tools (Scripps Research Institute, La Jolla, CA). The structures of the HBGA ligands were generated using the online *Glycam* molecular builder at http://glycam.ccrc.uga.edu/ccrc. Grid box parameters were assigned using the following procedure. Open Babel *obfit* command was used to align the fucose moiety in the ligand with that of **L23** in the crystal structure. The parameters of a minimal rectangular box, which accommodates the ligand, were expanded 2 Å in each direction. For each ligand, poses

were generated using Autodock Vina with an exhaustiveness set at 64 and arbitrary random seed values. Only poses for which the position of the L-fucose moiety matched (with RMSD < 1 Å) the position of that residue in the crystal structure and all inter-glycosidic dihedral angles were in agreement with exo-anomeric effect were considered (El-Hawiet et al. 2011). The resulting poses were then refined using MD simulations. The protein was protonated with *reduce* and its parameters and partial charges were assigned according to Amber2003 force field (*ff03.r1*) using *antechamber* and *sleap*. The assigning of AM1-BCC atomic charges for the ligands was conducted using the *sqm* module in Amber 11. The general Amber force field (GAFF) was used for the HBGA ligands. The ligands were placed in the binding site according to poses generated by docking. The resulting complex was neutralized by addition of $Na^+$ counter-ions and placed in a rectangular box of TIP3P water that extended 8 Å in all dimensions from the outer limits of the complex.

The MD simulations were performed using Amber 11 on a CentOS 6.0 computer. After minimization (first 1000 steps using steepest descent, then 1000 steps with the conjugate gradients with restrained solute (500 kcal $mol^{-1}Å^{-2}$)) the system was heated to 300 K with weak restraints to the solute (10 kcal $mol^{-1}Å^{-2}$) and equilibrated for 30 ps with controlled pressure and temperature. Each 200 ps production run was performed on partially constrained complex (amino acid residues that did not contact the ligand were restrained at 1 kcal $mol^{-1}Å^{-2}$) at 1 atm, 300 K using the Langevin heat bath with 1 $ps^{-1}$ collision frequency. Non-bonded interactions were evaluated with 8 Å cut off and the SHAKE constraint system for bonds to hydrogen was enabled. Long-range electrostatic interactions were treated with particle-mesh Ewald (PME)

periodic boundary conditions.

The larger HBGA ligands (**L2-L11**, **L13-L22**, **L24-L33**, **L35 and L37-L41**) were modeled based on the structure of the smallest member of the congeneric series, the corresponding disaccharide for the H antigens and trisaccharide for the A, B and Lewis antigens. Putative bound poses of each of larger congeners were prepared by superimposing their atomic coordinates with the atomic coordinates of the corresponding di- or trisaccharide template in the complex. To alleviate possible clashes with the protein, the ligand position was adjusted using a local search method in Autodock Vina. The resulting structure was then subjected to MD simulations, as described above.

**Results and Discussion**

**HBGA affinities**

The direct ESI-MS assay was carried out to test for specific binding between the P dimer and the truncated P dimer and each of the 41 HBGA oligosaccharides and to quantify their affinities at pH 7 and 25 °C. Shown in Figure 1 are ESI mass spectra acquired for an aqueous ammonium acetate (10 mM) solution of the P dimer (12 μM) and of the truncated P dimer (12 μM). From the mass spectra it can be seen that the recombinant NoV VA387 P domain exists predominantly as a dimer (i.e., $P_2$) under these solution conditions, with only protonated $P_2^{n+}$ ions detected. The measured MW of 69,312 ± 2 Da of the P dimer is in good agreement with the theoretical value of 69,311 Da. The truncated P domain also forms a dimer (i.e., tr-$P_2$) under these conditions. However, the mass spectrum reveals evidence of three different protein species. In addition to signal for the protonated ions (tr-$P_2^{n+}$) of the expected tr-$P_2$ (measured MW of 69,004 ± 2 Da,

theoretical MW 69,006 Da), ions corresponding to protonated ions of proteins with MW of 68,763 ± 8 Da and 69,160 ± 10 Da were detected. As illustrated in Figure S3, the three isoforms of tr-$P_2$ exhibit similar affinities for the HBGA.

Shown in Figure 2 are typical ESI mass spectra measured for aqueous ammonium acetate solutions (10 mM) with P dimer (12 μM) and 20, 70 and 100 μM A type 6 tetrasaccharide (**L17**), respectively. The scFv (10 μM), which served as $P_{ref}$, was present in all of the ESI solutions used for affinity measurements. According to the ESI-MS data, the P dimer binds up to two molecules of **L17**, i.e., $(P_2 + q\mathbf{L17})^{n+}$, where $q$ = 0 - 2 and n = 15 - 18. Signals corresponding to unbound and bound $P_{ref}$ ions were also detected, i.e., $(P_{ref} + q\mathbf{L17})^{n+}$, where $q$ = 0 - 2 and n = 9 - 11, which indicates that nonspecific binding of P dimer to **L17** occurred during the ESI process. As seen in Figures 2d-f, after correction for nonspecific binding, no ions corresponding to specific ($P_2$ + *2***L17**) complex were identified (El-Hawiet et al. 2011). Therefore, the P dimer binds to a single molecule of **L17** under these solution conditions, with a $K_a$ of 2400 ± 150 $M^{-1}$. A summary of the $K_a$ values obtained for the P dimer binding to each of the 41 HBGA oligosaccharides is listed in Table I.

Because the interactions between the P dimer and the HBGA oligosaccharides are quite weak, it was desirable to establish the reliability of the ESI-MS binding protocol used for the measurements. To this end, ESI-MS titration experiments were carried out on a small number of HBGA oligosaccharides (**L6**, **L17** and **L28**, which represent H, A and B type 6 antigens) using a fixed P dimer concentration (12 μM) and seven or more different HBGA concentrations (10 – 120 μM). Figure 3 shows the plot of the fraction of **L17** bound P dimer ($R$/($R$+1)) versus **L17**

concentrations and the curve of fitting eq 4 to the experimental data (after correction for nonspecific binding). Non-linear fitting yields a $K_a$ value of 2350 ± 60 $M^{-1}$. In a similar way, $K_a$ value of 650 ± 50 $M^{-1}$ and 1200 ± 120 $M^{-1}$ were determined for ligands **L6** and **L28**, respectively. Notably, the affinities obtained from the titration experiments are in excellent agreement with the values obtained using a limited number of HBGA oligosaccharides at different concentrations.

As a further test the reliability of the ESI-MS assay, measurements were also performed on two human milk oligosaccharides (HMO), 3'-siallyllactose and 6'-siallyllactose, which were reported not to bind to the P dimer (Fiege et al. 2012). Figure S4 shows representative ESI mass spectra acquired for aqueous ammonium acetate solutions (10 mM) with P dimer (12 μM) and 60 μM of 3'-siallyllactose (**L42**) or 6'-siallyllactose (**L43**) and scFv (10 μM). Although there were signals corresponding to binding of each of the oligosaccharides to the P dimer, these were found to be due entirely to nonspecific binding.

The ESI-MS binding measurements revealed that the P dimer recognizes all HBGA oligosaccharides investigated. However, the binding is uniformly weak, ranging from ~400 to ~3000 $M^{-1}$. The highest affinity ligands for P dimer are B tetrasaccharide type 3 (**L26**) and A tetrasaccharide type 6 (**L17**), with $K_a$ values of 3000 ± 300 $M^{-1}$ and 2350 ± 60 $M^{-1}$, respectively. Interestingly, the affinities measured for the P dimer are similar in magnitude to that estimated for the VLP of another GII.4 NoV (Ast6139) (Fiege et al. 2012). Given that the P dimer only possesses two binding sites, while the VLP has 180 sites and assuming that the binding sites of the P dimer resembles those of the VLP, the apparent affinities of the VA387 VLP for these soluble oligosaccharides are expected to range from $10^4$ $M^{-1}$ to $10^6$ $M^{-1}$.

The binding data in Table I reveal that, overall, the A and B antigens bind more strongly to the P dimer than do the H and Lewis antigens. This finding appears to be consistent with the previously proposed NoV binding model, in which VA387 can recognize HBGAs through either a α-D-GalNAc or α-D-Gal epitope, and a α-L-Fuc epitope, using two different binding pockets (Figure 4) (Tan and Jiang 2005a). The A and B antigens possess both epitopes, which could be the reason for the stronger binding than those of the H and Lewis antigens, which lack the α-D-GalNAc/α-D-Gal epitope. The binding data also indicate that both 1,2-linked α-L-Fuc (H epitope) and 1,3/4-linked α-L-Fuc ($Le^a$ and $Le^X$ epitope) are recognized by the P dimer with comparable affinities.

The present data also indicate that the precursor chain type influences the strength of HBGA binding. For the H antigens, type 3 displays higher affinity over the remaining types 1, 2, 4, 5 and 6, which exhibit similar affinities ranging from 400 to 700 $M^{-1}$. The finding that type 2 binds with comparable affinity as 1, 4, 5 and 6 is in agreement with results determined by the STD-NMR spectroscopy reported by Peters and coworkers (Fiege et al. 2012). However, this is inconsistent with those measured by the ELISA, which suggested that VA387 VLP does not bind to H type 2 trisaccharide (Huang et al. 2005). For the A antigens, type 6 exhibits the strongest, type 2 the weakest; while types 1, 3, 4 and 5 exhibit similar affinities ranging from 1200 to 1600 $M^{-1}$. For the B antigens, type 3 displays the highest affinity, and similar to the A antigens, type 2 the weakest; while types 1, 4, 5 and 6 exhibit similar affinities (in the range of 1100 to 1400 $M^{-1}$).

The affinities of the truncated P dimer for the 41 listed HBGAs were also measured (Table I). Overall, they are similar in magnitude to those measured for the P dimer. These results

indicate that elimination of the C-terminal arginine tail, which is remote from the binding pocket, does not influence substantially the binding of the P domain with the HBGAs. This finding contrasts the results of a previous study, which suggested that the removal of arginine tail eliminated binding to the HBGA (Tan et al. 2006).

**Docking analysis**

To further elucidate the influence of structure of the HBGA on the strength of their interactions with the P dimer, molecular docking analysis was performed on each of the HBGA oligosaccharides investigated. The results of this analysis are summarized below.

*H antigens*

Docking analysis revealed that all of the H antigens (**L1-L11**) share a common binding motif comprising the α-L-Fuc-(1→2)-β-D-Gal disaccharide. In each case, the α-L-Fuc residue engages in hydrogen bonds (H-bonds) with T344, R345, D374 of chain A and G442' of chain B, while the β-D-Gal residue forms H-bonds with residues D391' and S441' in chain B (Figure S5). Atomic coordinates derived from the energy optimized structures of type H oligosaccharides docked into binding site of NoV VA387 P dimer are given in the Supplementary Data file docking_H_pdb.rar. With the exception of the type 3, additional H-bonds were identified for the H antigen trisaccharides. However, as noted above, the P dimer exhibits the highest affinity for type 3 H antigen. Therefore, it would seem that these putative stabilizing interactions do not significantly enhance binding. Docking of the larger oligosaccharides leads to a similar conclusion – there is no obvious correlation between the number of putative H-bonds identified in the docking results and the measured affinities.

*A and B antigens*

As described above, the P dimer exhibits, with a few exceptions, higher affinities for the A and B antigens compared to the H antigen. These findings can be reasonably explained by the participation of the α-D-GalNAc (A antigens) or α-D-Gal (B antigen) residues in binding interactions, in addition to those involving the α-L-Fuc-(1→2)-β-D-Gal moiety. According to the docking results for the A antigens (Figure S5 and Supplementary Data file docking_A_pdb.rar), the α-D-GalNAc residue of the A antigens forms H-bonds with residues K348' and S441' (chain B). Moreover, residue I389' (chain B) may engage in van der Waals interactions with the N-acetyl group of terminal α-D-GalNAc. The docking results for the B antigens (Figure S5, and Supplementary Data file docking_B_pdb.rar) reveal that the α-D-Gal residue forms H-bonds with residues A346 (chain A) and Q331', K348', S441' (chain B). As was the case for the H antigens, additional H-bonds were identified for some of the larger A and B oligosaccharides. However, these putative interactions do not translate to significant changes in affinity.

*Lewis antigens*

The Lewis structures are characterized by the Lewis epitope (i.e., 1,3-linked α-L-Fuc in $Le^X$ and $Le^Y$ antigens or 1,4-linked α-L-Fuc in $Le^a$ and $Le^b$ antigens). Although lacking the central binding motif, the α-L-Fuc-(1→2)-β-D-Gal disaccharide, the $Le^X$ and $Le^a$ antigens nevertheless bind to the P dimer with affinities similar to those of the H antigens. From the docking analysis (Figure S5, and Supplementary Data file docking_Lewis_pdb.rar), the 1,3/4-linked α-L-Fuc residue in $Le^X$ and $Le^a$ antigens is able to form H-bonds with residues T344, R345, D374 (chain A) and G442' (chain B). In addition, the β-D-GlcNAc residue forms H-bonds to residues S441'

and D391' (chain B). The $Le^Y$ and $Le^b$ antigens possess both the α-L-Fuc-(1→2)-β-D-Gal and 1,3/4-linked α-L-Fuc motifs, both of which are recognized by the protein. However, the docking results indicate that the P dimer binds preferentially to the 1,3/4-linked α-L-Fuc motif (Figure S5, and Supplementary Data file docking_Lewis_pdb.rar). The 1,3/4-linked α-L-Fuc residue in $Le^Y$ and $Le^b$ antigens forms H-bonds with residues T344, R345, D374 (chain A) and G442' (chain B). For the $Le^Y$ antigens, the β-D-GlcNAc residue also interacts with residue D391' (chain B). This interaction is not present for the $Le^b$ antigens; instead, the 1,2-linked α-L-Fuc residue interacts with residue G392' (chain B).

**Conclusion**

In summary, the interactions between the NoV VA387 P dimer and a truncated P dimer with a library of 41 HBGA oligosaccharides were quantified for the first time. The results of the binding measurements performed at 25 °C and pH 7 indicate that the P dimer binds to all of the HBGA oligosaccharides with affinities ranging from 400 to 3000 $M^{-1}$. The affinities of the truncated P dimer, which lacks the Arg-cluster at the C-terminus, for the HBGAs are similar in magnitude to those measured for the P dimer. Based on the affinities measured for the P dimer, the apparent affinities of NoV VA387 for the HBGA are estimated between $10^4$ and $10^6$ $M^{-1}$. Efforts are now underway in our laboratory to quantify directly the affinities of the VA387 VLP, as well as the corresponding P particle, for the HBGA oligosaccharides.

Overall, the P dimer exhibits higher affinities for the A and B antigens compared to those of the H and Lewis antigens. This finding is consistent with a proposed norovirus binding model, in which VA387 can recognize HBGAs through both a α-D-GalNAc-(1→3)/α-D-Gal-(1→3)

epitope, and a α-L-Fuc(1→2) epitope, using two different binding sites. From the binding measurements, the influence of chain type on the affinities was found to be: 3 > 1 ≈ 2 ≈ 4 ≈ 5 ≈ 6 for H antigens; 6 > 1 ≈ 3 ≈ 4 ≈ 5 > 2 for A antigens; 3 > 1 ≈ 4 ≈ 5 ≈ 6 > 2 for B antigens. The central binding motifs in the HBGAs were identified from molecular docking simulations. However, the modeling did not reveal the structural basis for the influence of chain type on the measured affinities.

**Supplementary Data**

Supplementary data for this article are available online at http://glycob.oxfordjounals.org/

**Acknowledgements**

The authors thank the Alberta Glycomics Centre (AGC) and the Natural Sciences and Engineering Research Council (NSECR) for supporting this research and Prof. Todd Lowary (University of Alberta) and Alberta Innovates Technology Futures for generously providing carbohydrate ligands used in this work. L.H also acknowledges an Alberta Innovates Graduate Student Scholarship and X.J. and M. T. acknowledge support from the National Institutes of Health of the Unites States of America.

**Abbreviations**

ESI-MS, electrospray ionization mass spectrometry; NoV, norovirus; HBGA, histo-blood group antigens; $K_a$, association constant; VLP, virus-like particle; STD-NMR, saturation transfer difference nuclear magnetic resonance; $P_2$, P dimer; tr-$P_2$, truncated P dimer; scFv, single chain variable fragment; $P_{ref}$, reference protein; *Ab*, abundance of gas-phase ions; Fuc, fucose; Gal, galactose; Glc, glucose; GalNAc, N-acetyl galactosamine; GlcNAc, N-acetyl glucosamine;

Neu5Ac, N-acetyl neuraminic acid; MD, molecular dynamics.

**References**

Bagal D, Kitova EN, Liu L, El-Hawiet A, Schnier PD, Klassen JS. 2009. Gas phase stabilization of noncovalent protein complexes formed by electrospray ionization. *Anal Chem*. 81:7801-7806.

Baert L, Mattison K, Loisy-Hamon F, Harlow J, Martyres A, Lebeau B, Stals A, Van Coillie E, Herman L, Uyttendaele M. 2011. Review: norovirus prevalence in Belgian, Canadian and French fresh produce: a threat to human health? *Int J Food Microbiol*. 151:261-269.

Bereszczak JZ, Barbu IM, Tan M, Xia M, Jiang X, van Duijn E, Heck AJR. 2012. Structure, stability and dynamics of norovirus P domain derived protein complexes studied by native mass spectrometry. *J Struct Biol*. 177:273-282.

Bu W, Mamedova A, Tan M, Xia M, Jiang X, Hegde RS. 2008. Structural basis for the receptor binding specificity of Norwalk virus. *J Virol*. 82:5340-5347.

Cannon JL, Lindesmith LC, Donaldson EF, Saxe L, Baric RS, Vinje J. 2009. Herd immunity to GII.4 noroviruses is supported by outbreak patient sera. *J Virol*. 83:5363-5374.

Cao S, Lou Z, Tan M, Chen Y, Liu Y, Zhang Z, Zhang XC, Jiang X, Li X, Rao Z. 2007. Structural basis for the recognition of blood group trisaccharides by norovirus. *J Virol*. 81:5949-5957.

Chen Y, Tan M, Xia M, Hao N, Zhang XC, Huang P, Jiang X, Li X, Rao Z. 2011. Crystallography of a Lewis-binding norovirus, elucidation of strain-specificity to the polymorphic human histo-blood group antigens. *PLoS Pathog*. 7:e1002152.

Choi JM, Hutson AM, Estes MK, Prasad BVV. 2008. Atomic resolution structural

characterization of recognition of histo-blood group antigens by Norwalk virus. *Proc Natl Acad Sci U S A*. 105:9175-9180.

Daniel JM, Friess SD, Rajagopalan S, Wendt S, Zenobi R. 2002. Quantitative determination of noncovalent binding interactions using soft ionization mass spectrometry. *Int J Mass Spectrom*. 216:1-27.

Deng L, Sun N, Kitova EN, Klassen JS. 2010. Direct quantification of protein-metal ion affinities by electrospray ionization mass spectrometry. *Anal Chem*. 82:2170-2174.

de Rougemont A, Ruvoen-Clouet N, Simon B, Estienney M, Elie-Caille C, Aho S, Pothier P, Le Pendu J, Boireau W, Belliot G. 2011. Qualitative and quantitative analysis of the binding of GII.4 norovirus variants onto human blood group antigens. *J Virol*. 85:4057-4070.

El-Hawiet A, Kitova EN, Kitov PI, Eugenio L, Ng KKS, Mulvey GL, Dingle TC, Szpacenko A, Armstrong GD, Klassen JS. 2011. Binding of *Clostridium difficile* toxins to human milk oligosaccharides. *Glycobiology*. 21:1217-1227.

Fiege B, Rademacher C, Cartmell J, Kitov PI, Parra F, Peters T. 2012. Molecular details of the recognition of blood group antigens by a human norovirus as determined by STD NMR spectroscopy. *Angew Chem Int Ed*. 51:928-932.

Greenberg HB, Valdesuso JR, Kalica AR, Wyatt RG, McAuliffe VJ, Kapikian AZ, Chanock RM. 1981. Proteins of Norwalk virus. *J Virol*, 37:994-999.

Hansman GS, Shahzad-ul-Hussan S, McLellan JS, Chuang G-Y, Georgiev I, Shimoike T, Katayama K, Bewley CA, Kwong PD. 2012. Structural basis for norovirus inhibition and fucose mimicry by citrate. *J Virol*. 86:284-292.

Hardy ME, White LJ, Ball JM, Estes MK. 1995. Specific proteolytic cleavage of recombinant Norwalk virus capsid protein. *J Virol*. 69:1693-1698.

Huang P, Farkas T, Marionneau S, Zhong W, Ruvoen-Clouet N, Morrow AL, Altaye M, Pickering LK, Newburg DS, LePendu J, Jiang X. 2003. Noroviruses bind to human ABO, Lewis, and secretor histo-blood group antigens: Identification of 4 distinct strain-specific patterns. *J Infect Dis*. 188:19-31.

Huang P, Farkas T, Zhong W, Thornton S, Morrow AL, Jiang X. 2005. Norovirus and histo-blood group antigens: demonstration of a wide spectrum of strain specificities and classification of two major binding groups among multiple binding patterns. *J Virol*. 79:6714-6722.

Jiang X, Wang M, Graham DY, Estes MK. 1992. Expression, self-assembly, and antigenicity of the Norwalk virus capsid protein. *J Virol*. 66:6527-6532.

Johnston CP, Qiu H, Ticehurst JR, Dickson C, Rosenbaum P, Lawson P, Stokes AB, Lowenstein CJ, Kaminsky M, Cosgrove SE, Green KY, Perl TM. 2007. Outbreak management and implications of a nosocomial norovirus outbreak. *Clin Infect Dis*. 45:534-540.

Kitova EN, El-Hawiet A, Schnier PD, Klassen JS. 2012. Reliable determinations of protein-ligand interactions by direct ESI-MS measurements. Are we there yet? *J Am Soc Mass Spectrom*. 23:431-441.

Lindesmith L, Moe C, Marionneau S, Ruvoen N, Jiang X, Lindbland L, Stewart P, LePendu J, Baric R. 2003. Human susceptibility and resistance to Norwalk virus infection. *Nat Med*. 9:548-553.

Meloncelli PJ, Lowary TL. 2009. Synthesis of ABO Type V and VI antigens. *Aust J Chem.*

62:558–574.

Meloncelli PJ, Lowary TL. 2010. Synthesis of ABO histo-blood group type I and II antigens. *Carbohydr Res*. 345:2304–2321.

Meloncelli PJ, West LJ, Lowary TL. 2011. Synthesis and NMR studies on the ABO histo-blood group antigens: synthesis of type III and IV structures and NMR characterization of type I–VI antigens. *Carbohydr Res.* 346:1406–1426.

Oriol R. 1990. Genetic-control of the fucosylation of ABH precursor chains - evidence for new epistatic interactions in different cells and tissues. *J Immunogenet*. 17:235-245.

Patel MM, Widdowson M-A, Glass RI, Akazawa K, Vinje J, Parashar UD. 2008. Systematic literature review of role of noroviruses in sporadic gastroenteritis. *Emerg Infect Dis.* 14:1224-1231.

Prasad BVV, Hardy ME, Dokland T, Bella J, Rossmann MG, Estes MK. 1999. X-ray crystallographic structure of the Norwalk virus capsid. *Science*. 286:287-290.

Ravn V, Dabelsteen E. 2000. Tissue distribution of histo-blood group antigens. *APMIS*. 108:1-28.

Sun J, Kitova EN, Klassen JS. 2007. Method for stabilizing protein-ligand complexes in nanoelectrospray ionization mass spectrometry. *Anal Chem*. 79:416-425.

Sun J, Kitova EN, Wang W, Klassen JS. 2006. Method for distinguishing specific from nonspecific protein-ligand complexes in nanoelectrospray ionization mass spectrometry. *Anal Chem*. 78:3010-3018.

Sun N, Soya N, Kitova EN, Klassen JS. 2010. Nonspecific interactions between proteins and charged biomolecules in electrospray ionization mass spectrometry. *J Am Soc Mass Spectrom*.

21:472-481.

Tan M, Fang P, Chachiyo T, Xia M, Huang P, Fang Z, Jiang W, Jiang X. 2008a. Noroviral P particle: structure, function and applications in virus-host interaction. *Virology*. 382:115-123.

Tan M, Fang P, Xia M, Chachiyo T, Jiang W, Jiang X. 2011a. Terminal modifications of norovirus P domain resulted in a new type of subviral particles, the small P particles. *Virology*. 410:345-352.

Tan M, Hegde RS, Jiang X. 2004. The P domain of norovirus capsid protein forms dimer and binds to histo-blood group antigen receptors. *J Virol*. 78:6233-6242.

Tan M, Huang P, Xia M, Fang PA, Zhong W, McNeal M, Wei C, Jiang W, Jiang X. 2011b. Norovirus P particle, a novel platform for vaccine development and antibody production. *J Virol*. 85:753-764.

Tan M, Jiang X. 2005a. Norovirus and its histo-blood group antigen receptors: an answer to a historical puzzle. *Trends Microbiol*. 13:285-293.

Tan M, Jiang X. 2005b. The P domain of norovirus capsid protein forms a subviral particle that binds to histo-blood group antigen receptors. *J Virol*. 79:14017-14030.

Tan M, Jiang X. 2007. Norovirus-host interaction: implications for disease control and prevention. *Expet Rev Mol Med*. 9:1-22.

Tan M, Jiang X. 2012. Norovirus P particle, a subviral nanoparticle for vaccine development against norovirus, rotavirus and influenza virus. *Nanomedicine*. 7:1-9.

Tan M, Meller J, Jiang X. 2006. C-terminal arginine cluster is essential for receptor binding of norovirus capsid protein. *J Virol*. 80:7322-7331.

Tan M, Xia M, Cao S, Huang P, Farkas T, Meller J, Hegde RS, Li X, Rao Z, Jiang X. 2008b. Elucidation of strain-specific interaction of a GII-4 norovirus with HBGA receptors by site-directed mutagenesis study. *Virology*. 379:324-334.

Tan M, Xia M, Chen Y, Bu W, Hegde RS, Meller J, Li X, Jiang X. 2009. Conservation of carbohydrate binding interfaces: evidence of human HBGA selection in norovirus evolution. *PLoS One*, 4:e5058.

Trott O, Olson AJ. 2010. Software news and update AutoDock Vina: improving the speed and accuracy of docking with a new scoring function, efficient optimization, and multithreading. *J Comput Chem*. 31:455-461.

Wang W, Kitova EN, Klassen JS. 2003. Influence of solution and gas phase processes on protein-carbohydrate binding affinities determined by nanoelectrospray Fourier transform ion cyclotron resonance mass spectrometry. *Anal Chem*. 75:4945-4955.

Yang Y, Xia M, Tan M, Huang P, Zhong W, Pang XL, Lee BE, Meller J, Wang T, Jiang X. 2010. Genetic and phenotypic characterization of GII-4 noroviruses that circulated during 1987 to 2008. *J Virol*. 84:9595-9607.

Zdanov A, Li Y, Bundle DR, Deng SJ, Mackenzie CR, Narang SA, Young NM, Cygler M. 1994. Structure of a single-chain antibody variable domain (Fv) fragment complexed with a carbohydrate antigen at 1.7-Å resolution. *Proc Natl Acad Sci U S A*. 91:6423-6427.

**Table I.** Apparent association constants, $K_a$ ($M^{-1}$) for binding of the HBGA oligosaccharides (**L1-L41**) and HMOs (**L42-L43**) with norovirus VA387 P dimer and truncated (tr) P dimer, measured at 25 °C and pH 7 by the direct ESI-MS assay.[a]

| | HBGA | | P dimer | tr-P dimer |
|---|---|---|---|---|
| **L1** | H disaccharide | α-L-Fuc-(1→2)-D-Gal | 470 ± 70 | 650 ± 60 |
| **L2** | H trisaccharide type 1 | α-L-Fuc-(1→2)-β-D-Gal-(1→3)-β-D-GlcNAc-$OC_8H_{15}$ | 500 ± 90 | 460 ± 70 |
| **L3** | H trisaccharide type 2 | α-L-Fuc-(1→2)-β-D-Gal-(1→4)-D-GlcNAc | 400 ± 50 | 300 ± 60 |
| **L4** | H trisaccharide type 3 | α-L-Fuc-(1→2)-β-D-Gal-(1→3)-α-D-GalNAc-$OC_8H_{15}$ | **1300 ± 130** | **1100 ± 300** |
| **L5** | H trisaccharide type 5 | α-L-Fuc-(1→2)-β-D-Gal-(1→3)-β-D-Gal-$OC_8H_{15}$ | 700 ± 100 | 790 ± 90 |
| **L6** | H trisaccharide type 6 | α-L-Fuc-(1→2)-β-D-Gal-(1→4)-D-Glc | 680 ± 70 [650 ± 50] [b] | 500 ± 110 |
| **L7** | H tetrasaccharide type 1 | α-L-Fuc-(1→2)-β-D-Gal-(1→3)-β-D-GlcNAc-(1→3)-D-Gal | 630 ± 30 | 850 ± 50 |
| **L8** | H tetrasaccharide type 2 | α-L-Fuc-(1→2)-β-D-Gal-(1→4)-β-D-GlcNAc-(1→4)-D-Gal | 420 ± 80 | 490 ± 60 |
| **L9** | H tetrasaccharide type 4 | α-L-Fuc-(1→2)-β-D-Gal-(1→3)-β-D-GalNAc-(1→3)-D-Gal | 570 ± 40 | 600 ± 100 |
| **L10** | H pentasaccharide type 1 | α-L-Fuc-(1→2)-β-D-Gal-(1→3)-β-D-GlcNAc-(1→3)-β-D-Gal-(1→4)-D-Glc | 610 ± 70 | 710 ± 80 |
| **L11** | H pentasaccharide type 2 | α-L-Fuc-(1→2)-β-D-Gal-(1→4)-β-D-GlcNAc-(1→3)-β-D-Gal-(1→4)-D-Glc | 500 ± 40 | 540 ± 80 |
| **L12** | A trisaccharide | α-D-GalNAc-(1→3)-[α-L-Fuc-(1→2)]-D-Gal | 850 ± 90 | 690 ± 30 |
| **L13** | A tetrasaccharide type 1 | α-D-GalNAc-(1→3)-[α-L-Fuc-(1→2)]-β-D-Gal-(1→3)-β-D-GlcNAc-$OC_8H_{15}$ | 1200 ± 130 | 1200 ± 200 |
| **L14** | A tetrasaccharide type 2 | α-D-GalNAc-(1→3)-[α-L-Fuc-(1→2)]-β-D-Gal-(1→4)-β-D-GlcNAc-$OC_8H_{15}$ | 570 ± 60 | 680 ± 80 |
| **L15** | A tetrasaccharide type 3 | α-D-GalNAc-(1→3)-[α-L-Fuc-(1→2)]-β-D-Gal-(1→3)-α-D-GalNAc-$OC_8H_{15}$ | 1600 ± 100 | 1100 ± 130 |
| **L16** | A tetrasaccharide type 5 | α-D-GalNAc-(1→3)-[α-L-Fuc-(1→2)]-β-D-Gal-(1→3)-β-D-Gal-$OC_8H_{15}$ | 1120 ± 80 | 1020 ± 50 |
| **L17** | A tetrasaccharide type 6 | α-D-GalNAc-(1→3)-[α-L-Fuc-(1→2)]-β-D-Gal-(1→4)-D-Glc | **2400 ± 150** [**2350 ± 60**] [b] | **1900 ± 160** |
| **L18** | A pentasaccharide type 1 | α-D-GalNAc-(1→3)-[α-L-Fuc-(1→2)]-β-D-Gal-(1→3)-β-D-GlcNAc-(1→3)-D-Gal | 1300 ± 100 | 830 ± 70 |

| | | | | |
|---|---|---|---|---|
| **L19** | A pentasaccharide type 2 | α-D-GalNAc-(1→3)-[α-L-Fuc-(1→2)]-β-D-Gal-(1→4)-β-D-GlcNAc-(1→3)-D-Gal | 560 ± 30 | 430 ± 90 |
| **L20** | A pentasaccharide type 4 | α-D-GalNAc-(1→3)-[α-L-Fuc-(1→2)]-β-D-Gal-(1→3)-β-D-GalNAc-(1→3)-D-Gal | 1040 ± 60 | 1000 ± 110 |
| **L21** | A hexasaccharide type 1 | α-D-GalNAc-(1→3)-[α-L-Fuc-(1→2)]-β-D-Gal-(1→3)-β-D-GlcNAc-(1→3)-β-D-Gal-(1→4)-D-Glc | 1200 ± 120 | 1200 ± 150 |
| **L22** | A hexasaccharide type 2 | α-D-GalNAc-(1→3)-[α-L-Fuc-(1→2)]-β-D-Gal-(1→4)-β-D-GlcNAc-(1→3)-β-D-Gal-(1→4)-D-Glc | 620 ± 70 | 530 ± 90 |
| **L23** | B trisaccharide | α-D-Gal-(1→3)-[α-L-Fuc-(1→2)]-β-D-Gal-$OC_2H_5$ | 1230 ± 90 | 1200 ± 200 |
| **L24** | B tetrasaccharide type 1 | α-D-Gal-(1→3)-[α-L-Fuc-(1→2)]-β-D-Gal-(1→3)-β-D-GlcNAc-$OC_8H_{15}$ | 1300 ± 200 | 1100 ± 200 |
| **L25** | B tetrasaccharide type 2 | α-D-Gal-(1→3)-[α-L-Fuc-(1→2)]-β-D-Gal-(1→4)-β-D-GlcNAc-$OC_8H_{15}$ | 820 ± 90 | 800 ± 110 |
| **L26** | B tetrasaccharide type 3 | α-D-Gal-(1→3)-[α-L-Fuc-(1→2)]-β-D-Gal-(1→3)-α-D-GalNAc-$OC_8H_{15}$ | **3000 ± 300** | **2400 ± 200** |
| **L27** | B tetrasaccharide type 5 | α-D-Gal-(1→3)-[α-L-Fuc-(1→2)]-β-D-Gal-(1→3)-β-D-Gal-$OC_8H_{15}$ | 1400 ± 260 | 1090 ± 90 |
| **L28** | B tetrasaccharide type 6 | α-D-Gal-(1→3)-[α-L-Fuc-(1→2)]-β-D-Gal-(1→4)-D-Glc | 1200 ± 90 [1200 ± 120] [b] | 1100 ± 100 |
| **L29** | B pentasaccharide type 1 | α-D-Gal-(1→3)-[α-L-Fuc-(1→2)]-β-D-Gal-(1→3)-β-D-GlcNAc-(1→3)-D-Gal | 1060 ± 70 | 1220 ± 60 |
| **L30** | B pentasaccharide type 2 | α-D-Gal-(1→3)-[α-L-Fuc-(1→2)]-β-D-Gal-(1→4)-β-D-GlcNAc-(1→3)-D-Gal | 780 ± 30 | 730 ± 90 |
| **L31** | B pentasaccharide type 4 | α-D-Gal-(1→3)-[α-L-Fuc-(1→2)]-β-D-Gal-(1→3)-β-D-GalNAc-(1→3)-D-Gal | 1320 ± 60 | 1200 ± 100 |
| **L32** | B hexasaccharide type 1 | α-D-Gal-(1→3)-[α-L-Fuc-(1→2)]-β-D-Gal-(1→3)-β-D-GlcNAc-(1→3)-β-D-Gal-(1→4)-D-Glc | 1400 ± 100 | 1300 ± 190 |
| **L33** | B hexasaccharide type 2 | α-D-Gal-(1→3)-[α-L-Fuc-(1→2)]-β-D-Gal-(1→4)-β-D-GlcNAc-(1→3)-β-D-Gal-(1→4)-D-Glc | 860 ± 60 | 820 ± 80 |
| **L34** | $Le^a$ trisaccharide | β-D-Gal-(1→3)-[α-L-Fuc-(1→4)]-D-GlcNAc | 360 ± 50 | 480 ± 70 |
| **L35** | $Le^a$ tetrasaccharide | β-D-Gal-(1→3)-[α-L-Fuc-(1→4)]-β-D-GlcNAc-(1→3)-D-Gal | 480 ± 40 | 590 ± 90 |
| **L36** | $Le^X$ trisaccharide | β-D-Gal-(1→4)-[α-L-Fuc-(1→3)]-D-GlcNAc | 550 ± 70 | 690 ± 80 |
| **L37** | $Le^X$ tetrasaccharide | β-D-Gal-(1→4)-[α-L-Fuc-(1→3)]-β-D-GlcNAc-(1→3)-D-Gal | 610 ± 50 | 670 ± 70 |
| **L38** | $Le^b$ tetrasaccharide | α-L-Fuc-(1→2)-β-D-Gal-(1→3)-[α-L-Fuc-(1→4)]-D-GlcNAc | 630 ± 70 | 590 ± 90 |
| **L39** | $Le^b$ pentasaccharide | α-L-Fuc-(1→2)-β-D-Gal-(1→3)-[α-L-Fuc-(1→4)]-β-D-GlcNAc-(1→3)-D-Gal | 500 ± 60 | 490 ± 60 |
| **L40** | $Le^Y$ tetrasaccharide | α-L-Fuc-(1→2)-β-D-Gal-(1→4)-[α-L-Fuc-(1→3)]-D-GlcNAc | 680 ± 40 | 690 ± 90 |

| | | | | |
|---|---|---|---|---|
| **L41** | $Le^Y$ pentasaccharide | α-L-Fuc-(1→2)-β-D-Gal-(1→4)-[α-L-Fuc-(1→3)]-β-D-GlcNAc-(1→3)-D-Gal | 490 ± 80 | 400 ± 70 |
| **L42** | 3'-siallyllactose | α-D-Neu5Ac-(2→3)-β-D-Gal-(1→4)-D-Glc | NB [c] | n.d. [d] |
| **L43** | 6'-siallyllactose | α-D-Neu5Ac-(2→6)-β-D-Gal-(1→4)-D-Glc | NB [c] | n.d. [d] |

a. Uncertainties correspond to one standard deviation. b. Values obtained from the ESI-MS titration experiments. c. NB = no binding detected. d. n.d. = not determined.

**Figure captions**

**Figure 1.** Direct ESI-MS analysis of norovirus VA387 P dimer and truncated P dimer at pH 7 and 25 °C. Representative mass spectra acquired for 10 mM ammonium acetate solution with (a) P dimer (12 μM) and (b) truncated P dimer (12 μM).

**Figure 2.** ESI mass spectra acquired in positive ion mode for aqueous ammonium acetate solutions (10 mM) at pH 7 and 25 °C containing norovirus VA387 P dimer (12 μM) and (a) 20 μM **L17** (A type 6 tetrasaccharide, MW 691 Da), (b) 70 μM **L17**, and (c) 100 μM **L17**. A $P_{ref}$ (10 μM) was added to each solution to correct the mass spectra for the occurrence nonspecific carbohydrate-protein binding during ESI process. Normalized distribution of **L17** (at concentrations of (d) 20 μM, (e) 70 μM and (f) 100 μM) bound to the P dimer before and after correcting the ESI mass spectra (shown in (a), (b) and (c)) for nonspecific ligand binding.

**Figure 3.** Fraction of ligand-bound P dimer (i.e., $R/(R+1)$) versus ligand concentration measured for **L6**, **L17** and **L28**, which represent H, A and B type 6 antigens. The titration experiments were carried out on aqueous ammonium acetate solutions (10 mM) at pH 7 and 25 °C containing P dimer (12 μM), $P_{ref}$ (10 μM) and ligand concentrations of between 10 and 120 μM. The solid curves correspond to the best fit of eq 4 to the experimental data for each ligand.

**Figure 4.** Interaction model for the norovirus VA387 P dimer binding to HBGA oligosaccharides adapted from the proposed model for norovirus-HBGA binding (Tan and Jiang 2005a). (a) Binding model proposed for A/B/H oligosaccharides;

illustrated by an A/B/H type 1 antigen. (b) Binding model proposed for Lewis oligosaccharides; illustrated by a $Le^b$ antigen. This model assumes that VA387 P dimer can accommodate both the H epitope and A/B epitope independently in two nearby binding pockets. In addition, the VA387 P dimer can also accommodate Lewis epitope in the H epitope binding pocket.

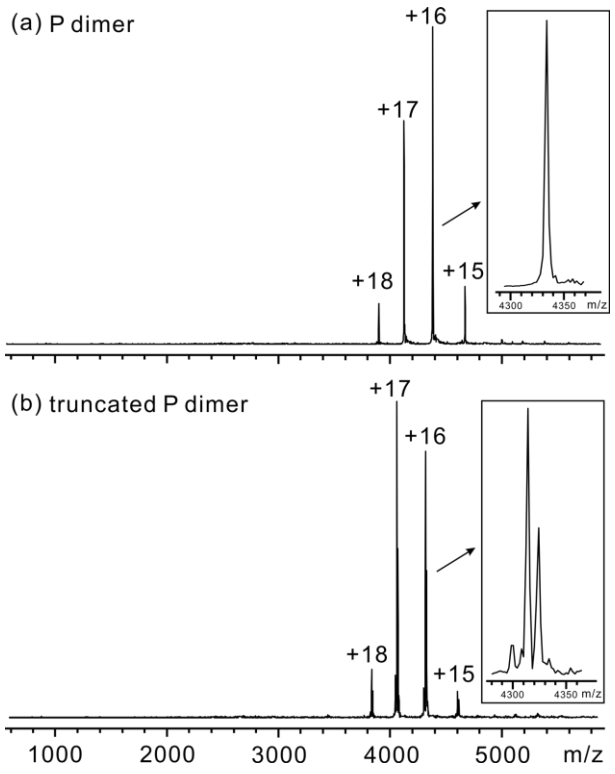
(a) P dimer
+16
+17
+18
+15
4300
4350 m/z
(b) truncated P dimer
+17
+16
+18
+15
4300
4350 m/z
1000
2000
3000
4000
5000
m/z

**Figure 1**

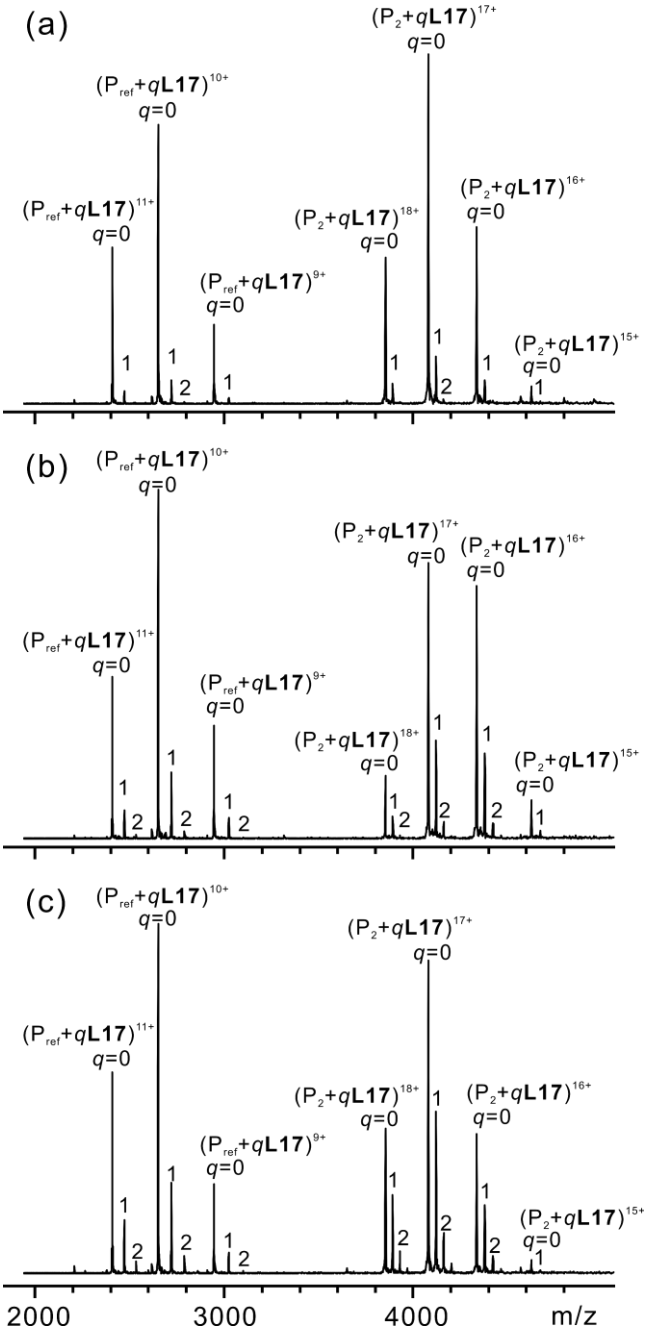
(a)
(P2+qL17)17+ q=0
(Pref+qL17)10+ q=0
(Pref+qL17)11+ q=0
(P2+qL17)18+ q=0
(P2+qL17)16+ q=0
(Pref+qL17)9+ q=0
(P2+qL17)15+ q=0
(b)
(Pref+qL17)10+ q=0
(P2+qL17)17+ q=0
(P2+qL17)16+ q=0
(Pref+qL17)11+ q=0
(Pref+qL17)9+ q=0
(P2+qL17)18+ q=0
(P2+qL17)15+ q=0
(c)
(Pref+qL17)10+ q=0
(P2+qL17)17+ q=0
(Pref+qL17)11+ q=0
(P2+qL17)18+ q=0
(P2+qL17)16+ q=0
(Pref+qL17)9+ q=0
(P2+qL17)15+ q=0
2000
3000
4000
m/z

**Figure 2**

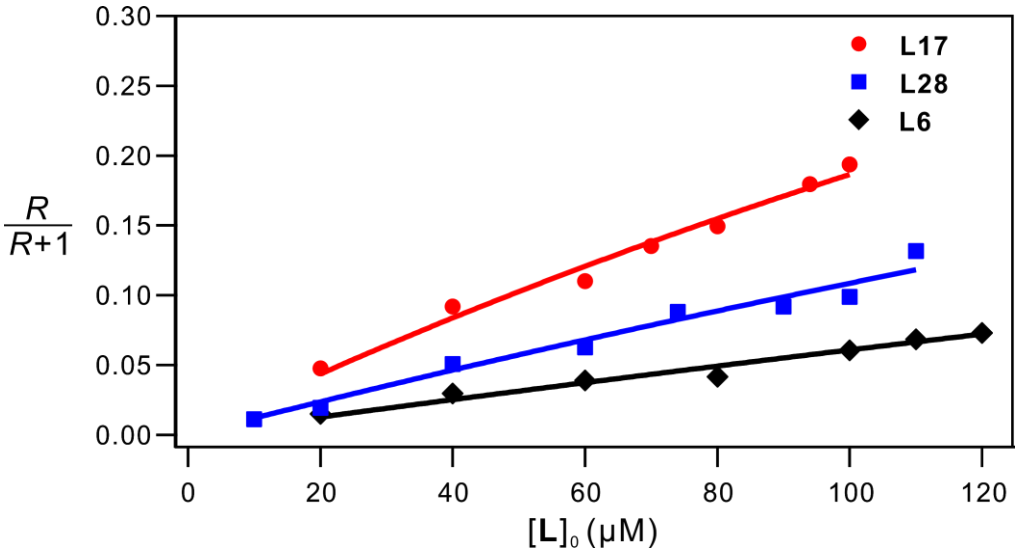
0.30
0.25
0.20
0.15
0.10
0.05
0.00
R/R+1
L17
L28
L6
0
20
40
60
80
100
120
[L]0 (μM)

**Figure 3**

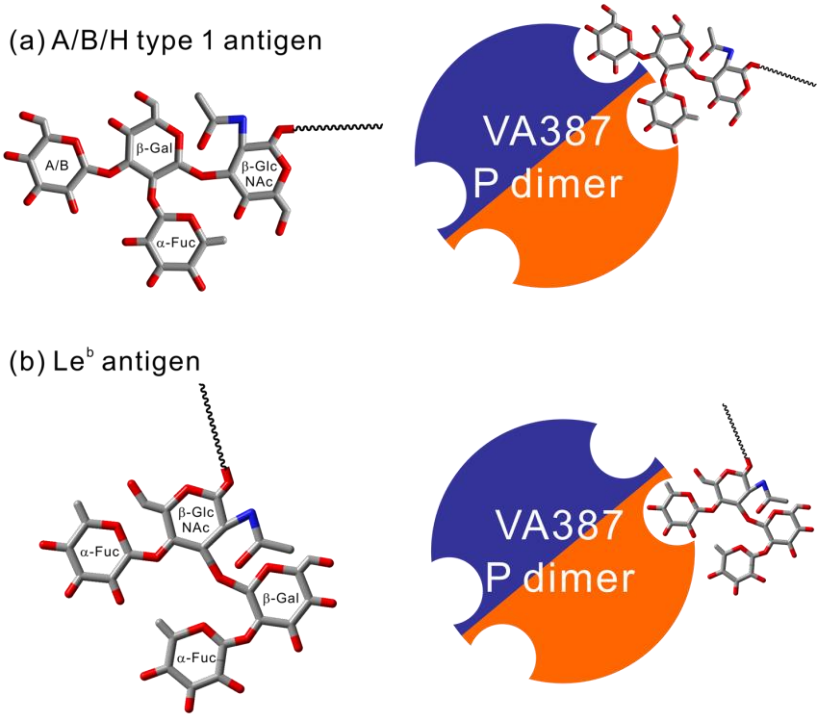
(a) A/B/H type 1 antigen
A/B
β-Gal
β-Glc NAc
α-Fuc
VA387
P dimer
(b) Le^b antigen
β-Glc NAc
α-Fuc
β-Gal
α-Fuc
VA387
P dimer

**Figure 4**

**Supplementary Materials**

**Affinities of Recombinant Norovirus P Dimer for Human Blood Group Antigens**

Ling Han, Pavel I. Kitov, Elena N. Kitova, Ming Tan, Leyi Wang, Ming Xia, Xi Jiang and John S. Klassen

**Figure S1.** Structures of the HBGA oligosaccharides.

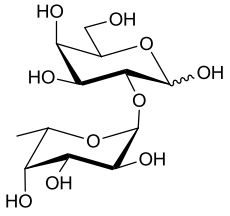

**L1**

H disaccharide

α-L-Fuc-(1→2)-D-Gal

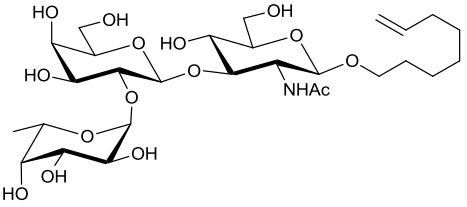

**L2**

H trisaccharide type 1

α-L-Fuc-(1→2)-β-D-Gal-(1→3)-β-D-GlcNAc-$OC_8H_{15}$

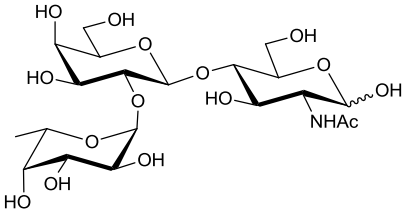

**L3**

H trisaccharide type 2

α-L-Fuc-(1→2)-β-D-Gal-(1→4)-D-GlcNAc

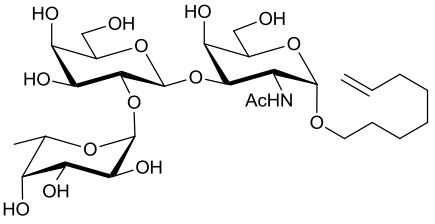

**L4**

H trisaccharide type 3

α-L-Fuc-(1→2)-β-D-Gal-(1→3)-α-D-GalNAc-$OC_8H_{15}$

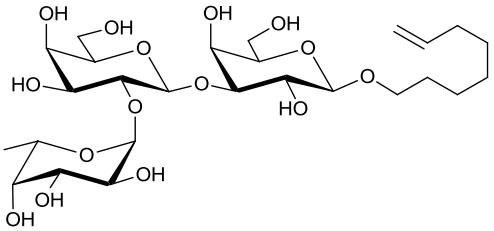

**L5**

H trisaccharide type 5

α-L-Fuc-(1→2)-β-D-Gal-(1→3)-β-D-Gal-$OC_8H_{15}$

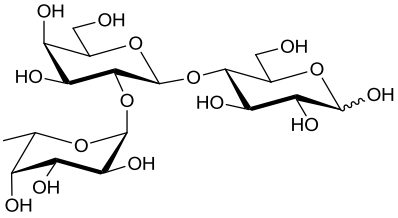

**L6**

H trisaccharide type 6

α-L-Fuc-(1→2)-β-D-Gal-(1→4)-D-Glc

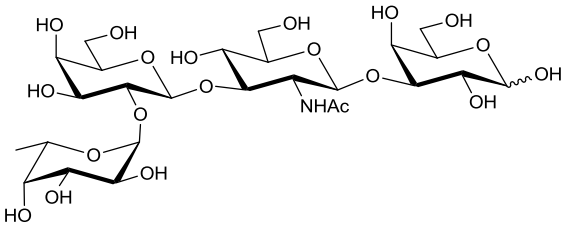

**L7**

H tetrasaccharide type 1

α-L-Fuc-(1→2)-β-D-Gal-(1→3)-β-D-GlcNAc-(1→3)-D-Gal

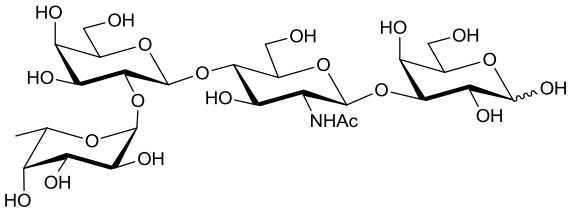

**L8**

H tetrasaccharide type 2

α-L-Fuc-(1→2)-β-D-Gal-(1→4)-β-D-GlcNAc-(1→4)-D-Gal

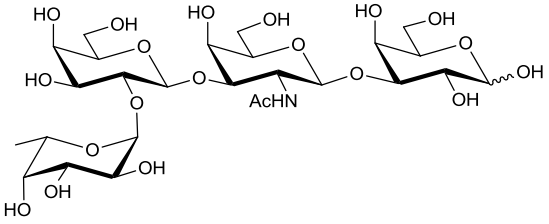

**L9**

H tetrasaccharide type 4

α-L-Fuc-(1→2)-β-D-Gal-(1→3)-β-D-GalNAc-(1→3)-D-Gal

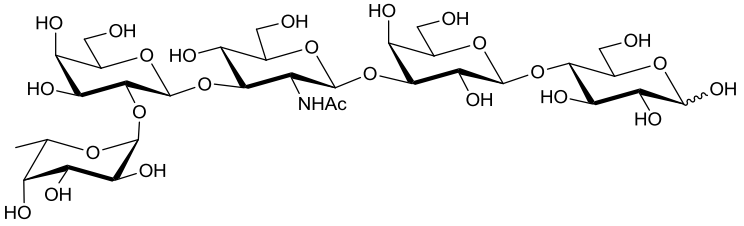

**L10**

H pentasaccharide type 1

α-L-Fuc-(1→2)-β-D-Gal-(1→3)-β-D-GlcNAc-(1→3)-β-D-Gal-(1→4)-D-Glc

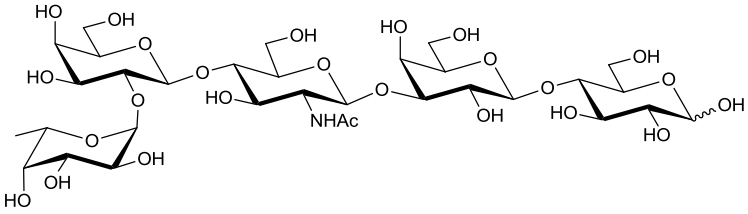

**L11**

H pentasaccharide type 2

α-L-Fuc-(1→2)-β-D-Gal-(1→4)-β-D-GlcNAc-(1→3)-β-D-Gal-(1→4)-D-Glc

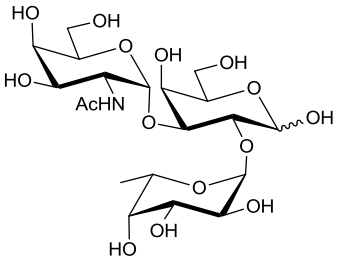

**L12**

A trisaccharide

α-D-GalNAc-(1→3)-[α-L-Fuc-(1→2)]-D-Gal

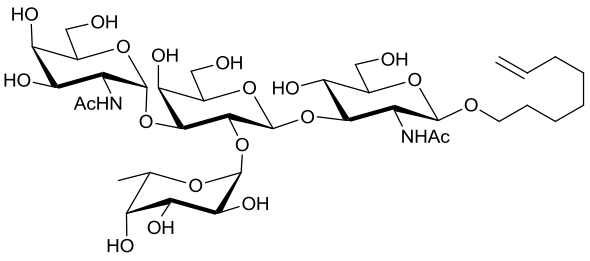

**L13**

A tetrasaccharide type 1

α-D-GalNAc-(1→3)-[α-L-Fuc-(1→2)]-β-D-Gal-(1→3)-β-D-GlcNAc-$OC_8H_{15}$

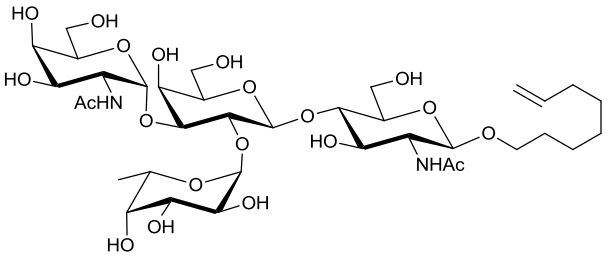

**L14**

A tetrasaccharide type 2

α-D-GalNAc-(1→3)-[α-L-Fuc-(1→2)]-β-D-Gal-(1→4)-β-D-GlcNAc-$OC_8H_{15}$

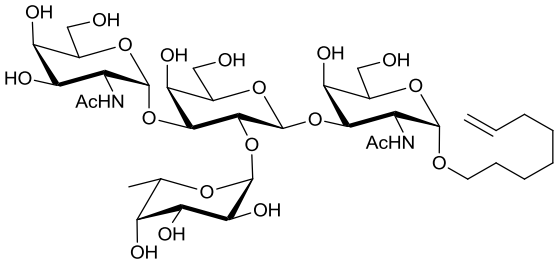

**L15**

A tetrasaccharide type 3

α-D-GalNAc-(1→3)-[α-L-Fuc-(1→2)]-β-D-Gal-(1→3)-α-D-GalNAc-$OC_8H_{15}$

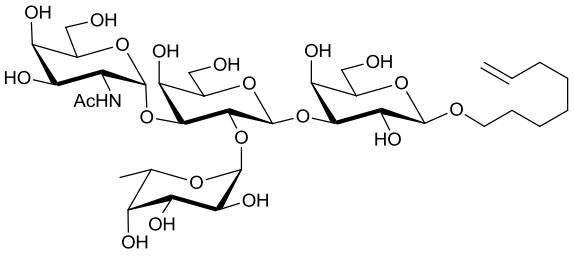

**L16**

A tetrasaccharide type 5

α-D-GalNAc-(1→3)-[α-L-Fuc-(1→2)]-β-D-Gal-(1→3)-β-D-Gal-$OC_8H_{15}$

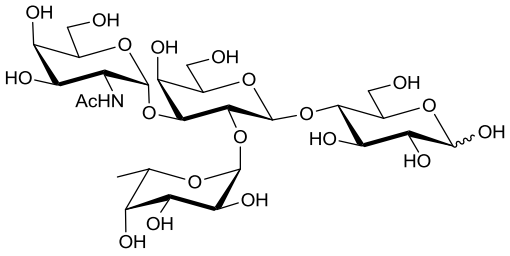

**L17**

A tetrasaccharide type 6

α-D-GalNAc-(1→3)-[α-L-Fuc-(1→2)]-β-D-Gal-(1→4)-D-Glc

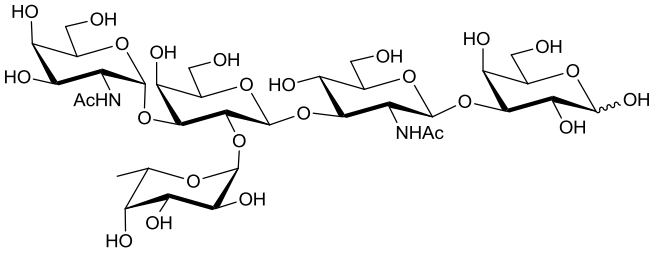

**L18**

A pentasaccharide type 1

α-D-GalNAc-(1→3)-[α-L-Fuc-(1→2)]-β-D-Gal-(1→3)-β-D-GlcNAc-(1→3)-D-Gal

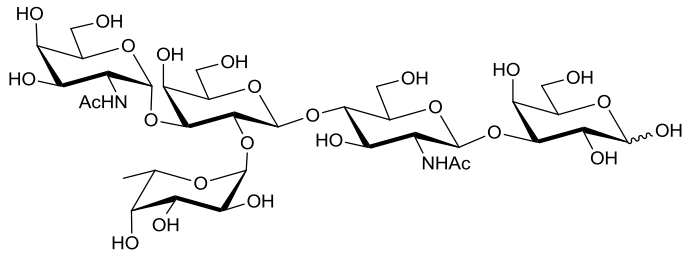

**L19**

A pentasaccharide type 2

α-D-GalNAc-(1→3)-[α-L-Fuc-(1→2)]-β-D-Gal-

(1→4)-β-D-GlcNAc-(1→3)-D-Gal

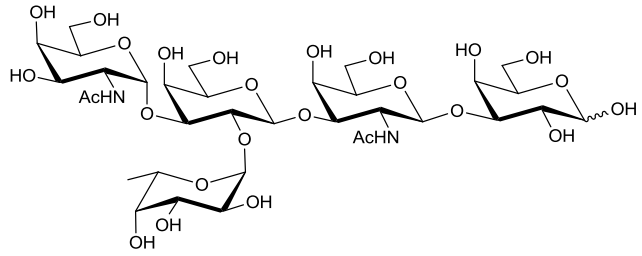

**L20**

A pentasaccharide type 4

α-D-GalNAc-(1→3)-[α-L-Fuc-(1→2)]-β-D-Gal-

(1→3)-β-D-GalNAc-(1→3)-D-Gal

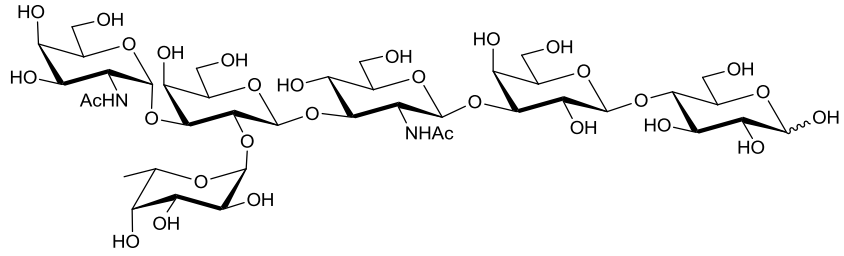

**L21**

A hexasaccharide type 1

α-D-GalNAc-(1→3)-[α-L-Fuc-(1→2)]-β-D-Gal-(1→3)-β-D-GlcNAc-

(1→3)-β-D-Gal-(1→4)-D-Glc

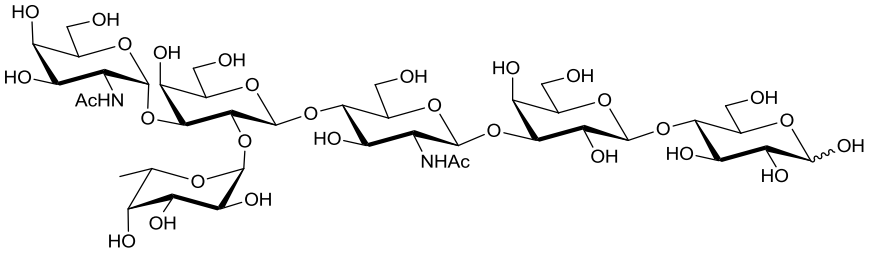

**L22**

A hexasaccharide type 2

α-D-GalNAc-(1→3)-[α-L-Fuc-(1→2)]-β-D-Gal-(1→4)-β-D-GlcNAc-(1→3)-β-D-Gal-(1→4)-D-Glc

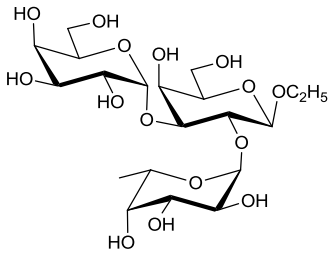

**L23**

B trisaccharide

α-D-Gal-(1→3)-[α-L-Fuc-(1→2)]-β-D-Gal-$OC_2H_5$

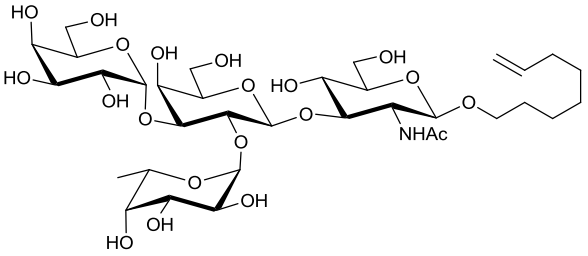

**L24**

B tetrasaccharide type 1

α-D-Gal-(1→3)-[α-L-Fuc-(1→2)]-β-D-Gal-(1→3)-β-D-GlcNAc-$OC_8H_{15}$

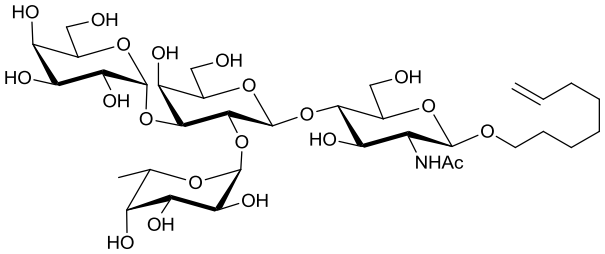

**L25**

B tetrasaccharide type 2

α-D-Gal-(1→3)-[α-L-Fuc-(1→2)]-β-D-Gal-(1→4)-β-D-GlcNAc-$OC_8H_{15}$

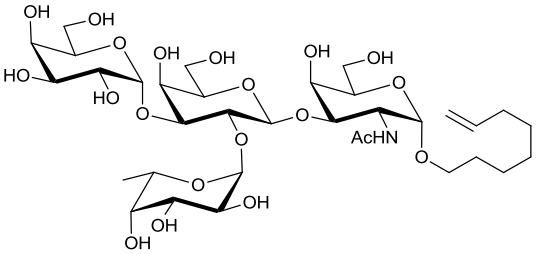

**L26**

B tetrasaccharide type 3

α-D-Gal-(1→3)-[α-L-Fuc-(1→2)]-β-D-Gal-(1→3)-α-D-GalNAc-$OC_8H_{15}$

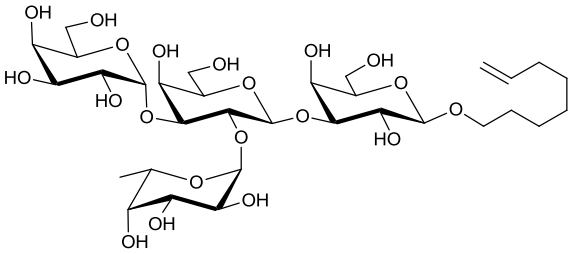

**L27**

B tetrasaccharide type 5

α-D-Gal-(1→3)-[α-L-Fuc-(1→2)]-β-D-Gal-(1→3)-β-D-Gal-$OC_8H_{15}$

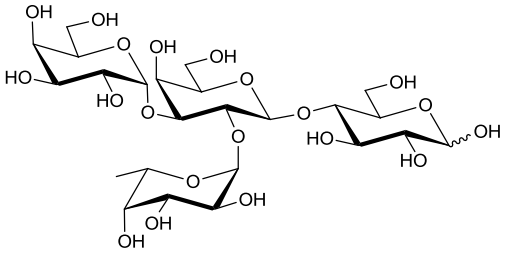

**L28**

B tetrasaccharide type 6

α-D-Gal-(1→3)-[α-L-Fuc-(1→2)]-β-D-Gal-(1→4)-D-Glc

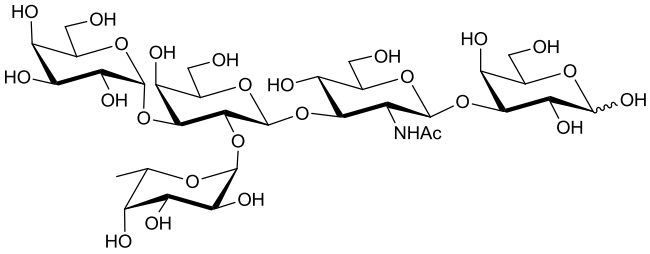

**L29**

B pentasaccharide type 1

α-D-Gal-(1→3)-[α-L-Fuc-(1→2)]-β-D-Gal-(1→3)-β-D-GlcNAc-(1→3)-D-Gal

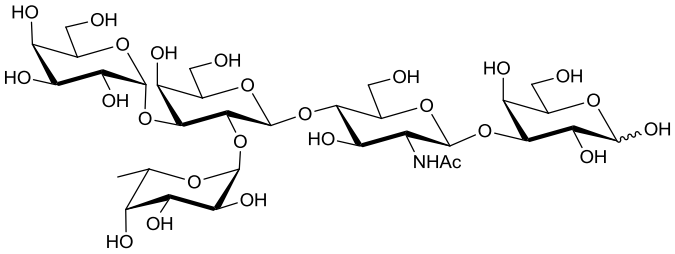

**L30**

B pentasaccharide type 2

α-D-Gal-(1→3)-[α-L-Fuc-(1→2)]-β-D-Gal-(1→4)-β-D-GlcNAc-(1→3)-D-Gal

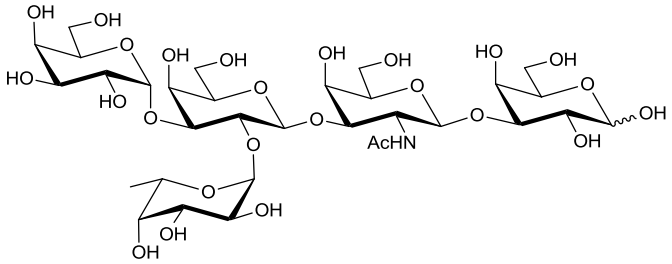

**L31**

B pentasaccharide type 4

α-D-Gal-(1→3)-[α-L-Fuc-(1→2)]-β-D-Gal-(1→3)-β-

D-GalNAc-(1→3)-D-Gal

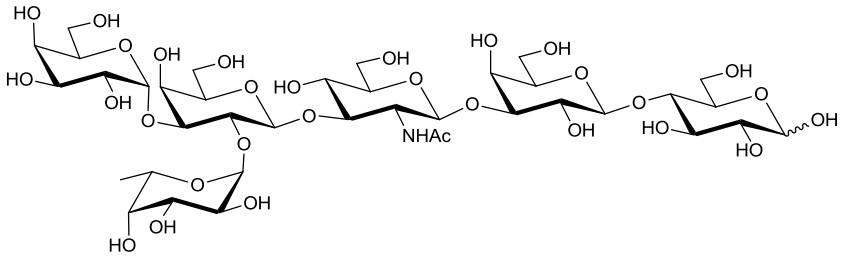

**L32**

B hexasaccharide type 1

α-D-Gal-(1→3)-[α-L-Fuc-(1→2)]-β-D-Gal-(1→3)-β-D-GlcNAc-(1→3)-

β-D-Gal-(1→4)-D-Glc

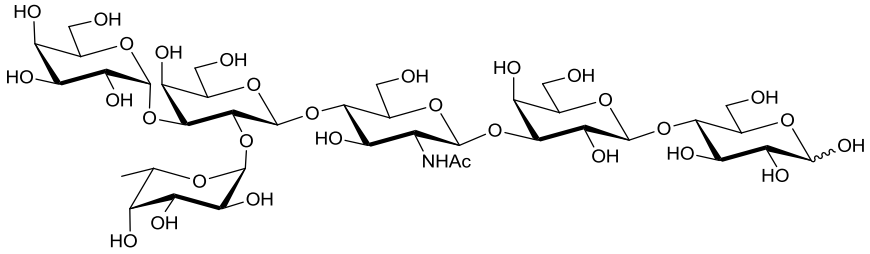

**L33**

B hexasaccharide type 2

α-D-Gal-(1→3)-[α-L-Fuc-(1→2)]-β-D-Gal-(1→4)-β-D-GlcNAc-(1→3)-

β-D-Gal-(1→4)-D-Glc

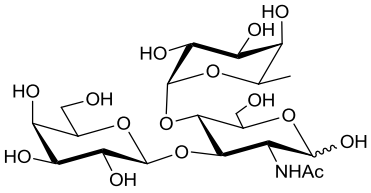

**L34**

Le[a] trisaccharide

β-D-Gal-(1→3)-[α-L-Fuc-(1→4)]-D-GlcNAc

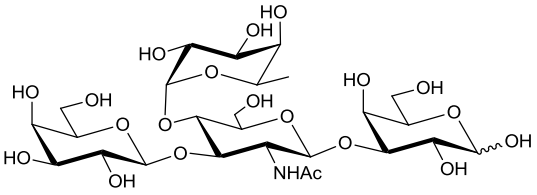

**L35**

Le[a] tetrasaccharide

β-D-Gal-(1→3)-[α-L-Fuc-(1→4)]-β-D-GlcNAc-(1→3)-D-Gal

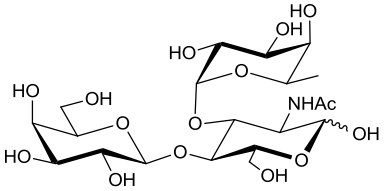

**L36**

Le[X] trisaccharide

β-D-Gal-(1→4)-[α-L-Fuc-(1→3)]-D-GlcNAc

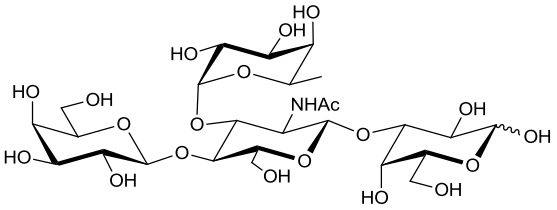

**L37**

Le[X] tetrasaccharide

β-D-Gal-(1→4)-[α-L-Fuc-(1→3)]-β-D-

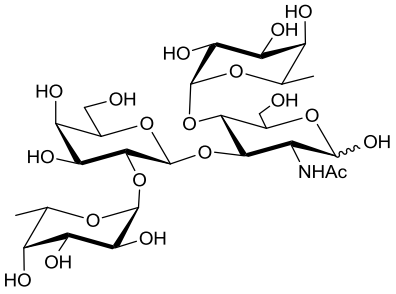

**L38**

Le[b] tetrasaccharide

α-L-Fuc-(1→2)-β-D-Gal-(1→3)-[α-L-Fuc-(1→4)]-D-GlcNAc

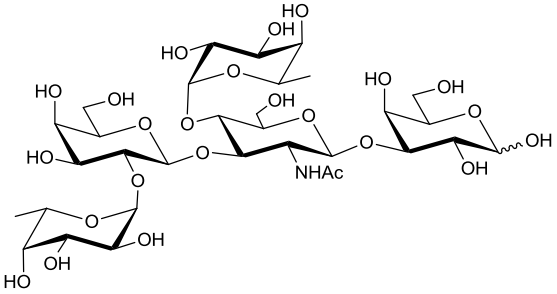

**L39**

Le[b] pentasaccharide

α-L-Fuc-(1→2)-β-D-Gal-(1→3)-[α-L-Fuc-(1→4)]-β-D-GlcNAc-(1→3)-D-Gal

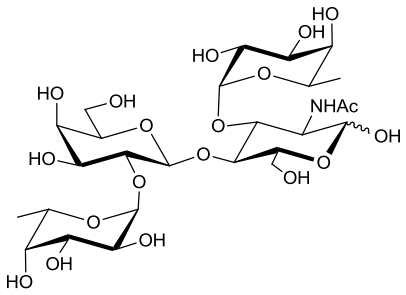

**L40**

Le$^{Y}$ tetrasaccharide

α-L-Fuc-(1→2)-β-D-Gal-(1→4)-[α-L-Fuc-(1→3)]-D-GlcNAc

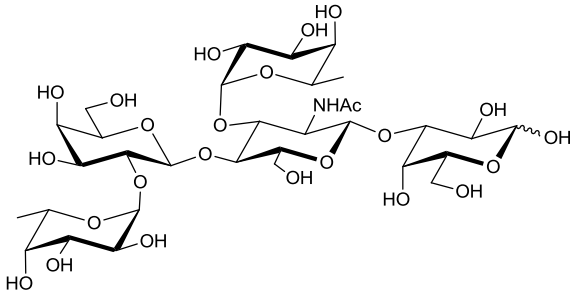

**L41**

Le$^{Y}$ pentasaccharide

α-L-Fuc-(1→2)-β-D-Gal-(1→4)-[α-L-Fuc-(1→3)]-β-D-GlcNAc-(1→3)-D-Gal

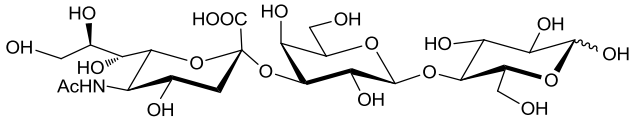

**L42**

3'-sialyllactose

α-D-Neu5Ac-(2→3)-β-D-Gal-(1→4)-D-Glc

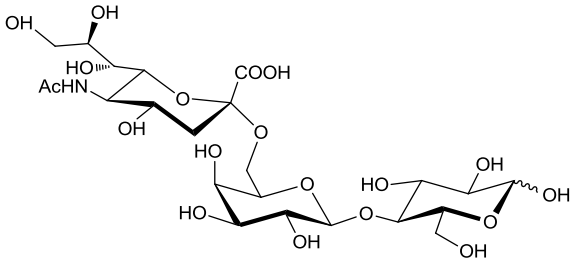

**L43**

6'-sialyllactose

**Figure S2.** (a) ESI mass spectrum acquired in positive ion mode for aqueous ammonium acetate (10 mM) solution at pH 7 and 25 °C containing norovirus VA387 tr-P dimer (12 μM), **L17** (40 μM), $P_{ref}$ (10 μM) and imidazole (10 mM). (b) Normalized distribution of **L17** bound to the P dimer after correction for nonspecific binding determined from the mass spectra. The calculated $K_a$ is 2300 ± 320 $M^{-1}$.

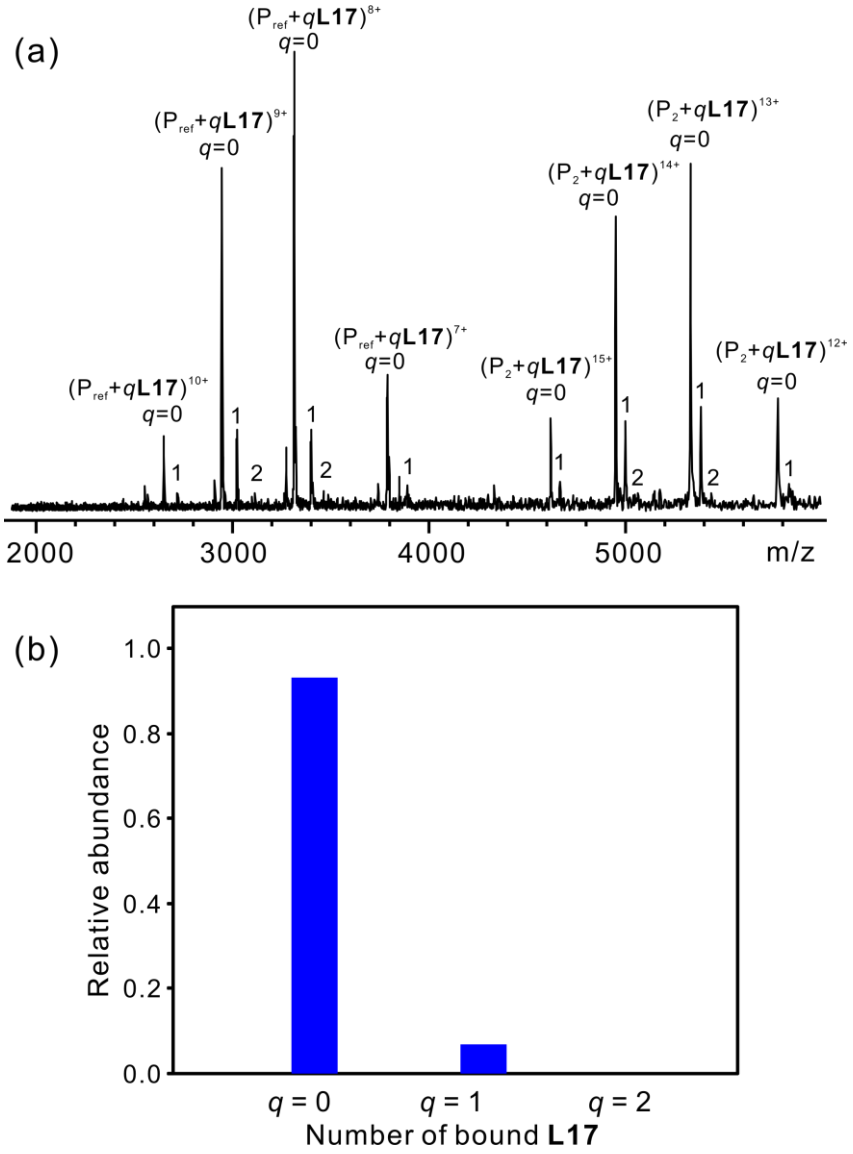

**Figure S3.** (a) ESI mass spectrum acquired in positive ion mode for aqueous ammonium acetate (10 mM) solution at pH 7 and 25 °C containing norovirus VA387 tr-P dimer (12 μM), **L26** (60 μM) and $P_{ref}$ (10 μM). (b) Normalized distributions of **L26** bound to the three tr-P dimer species (tr-$P_2$(I), tr-$P_2$(II) and tr-$P_2$(III)) after correction for nonspecific ligand binding determined from the mass spectrum shown in (a).

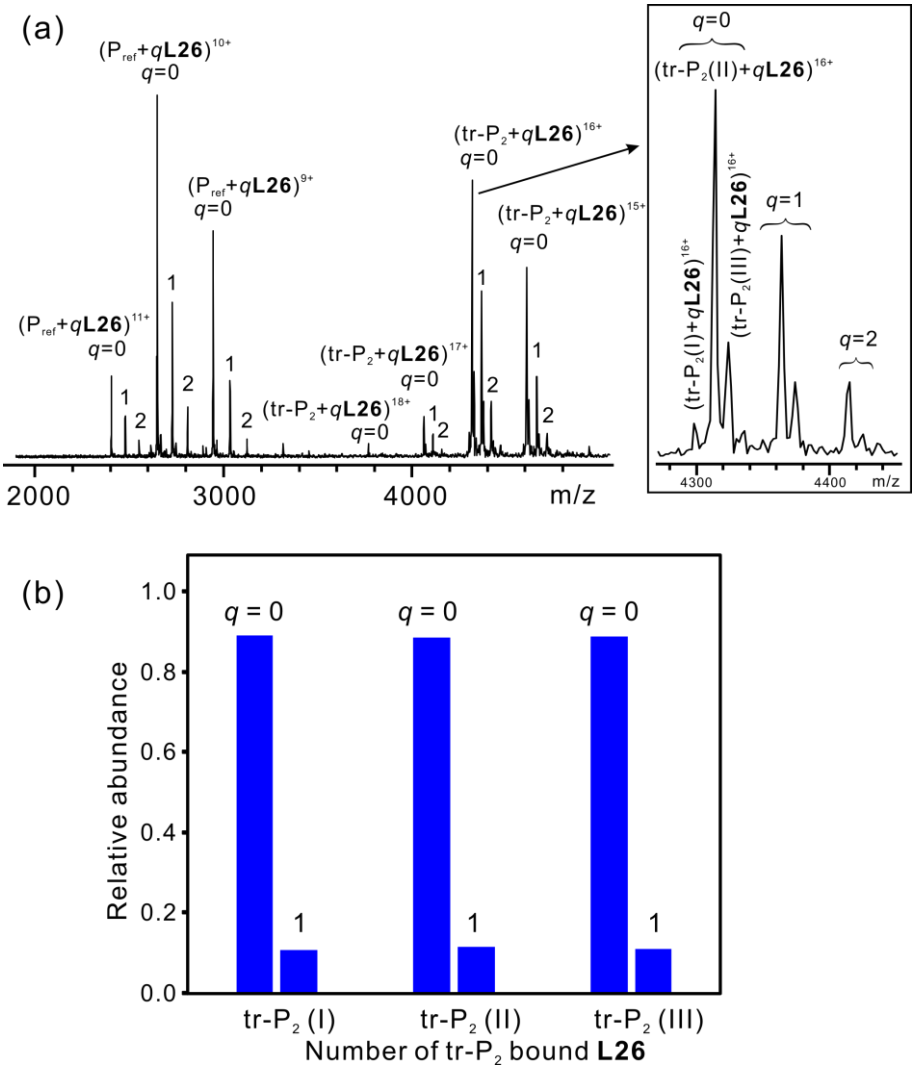

**Figure S4.** ESI mass spectra acquired in positive ion mode for aqueous ammonium acetate solutions (10 mM) at pH 7 and 25 °C containing norovirus VA387 P dimer (12 μM) and 60 μM (a) **L42** or (b) **L43**. A $P_{ref}$ (10 μM) was added to each solution to correct the mass spectra for the occurrence nonspecific carbohydrate-protein binding during the ESI process. Normalized distributions of (c) **L42** and (d) **L43** bound to the P dimer before and after correction for nonspecific binding determined from the mass spectra shown in (a) and (b), respectively.

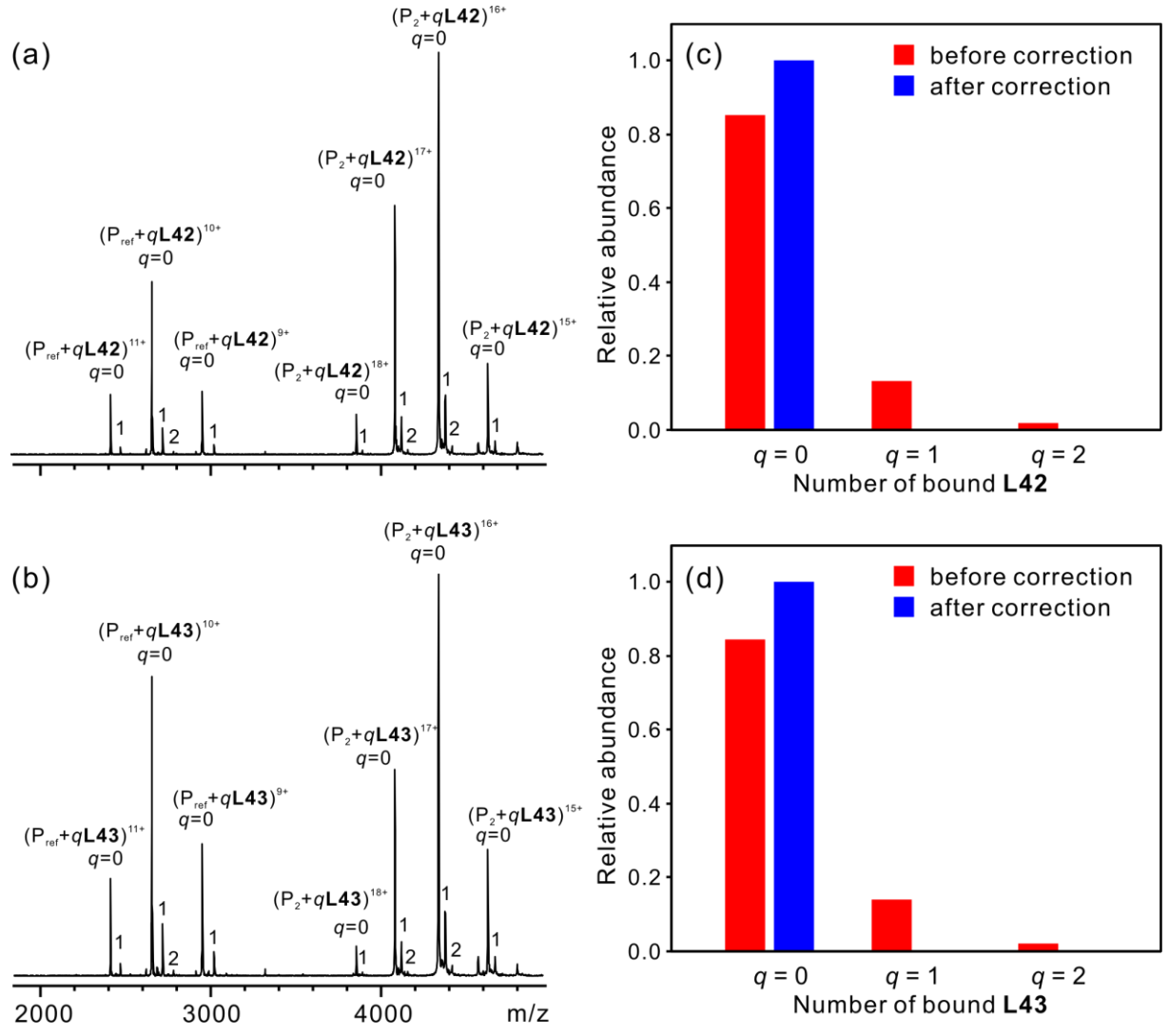

**Figure S5.** Molecular docking simulations for HBGA oligosaccharides binding to norovirus P domain using AutoDock Vina followed by energy minimization with molecular dynamic simulation using Amber. The crystal structure of the P domain of VA387 (GII.4 strain) bound to the B trisaccharide ligand (**L23**) was used as model of the P dimer binding site (pdb entry: 2obt). Representative poses are shown for type 1-6 H oligosaccharides (**L1**-**L11**); A oligosaccharides (**L12**-**L22**); and B oligosaccharides (**L23**-**L33**). The docking poses for Lewis oligosaccharides (**L34**, **L35**, **L36**, **L38**, **L39** and **L40**) are also shown. The dashed lines (yellow) indicate putative hydrogen bonds between the HBGA oligosaccharides and protein residues. PyMOL (http://www.pymol.org) was used to visualize the structures.

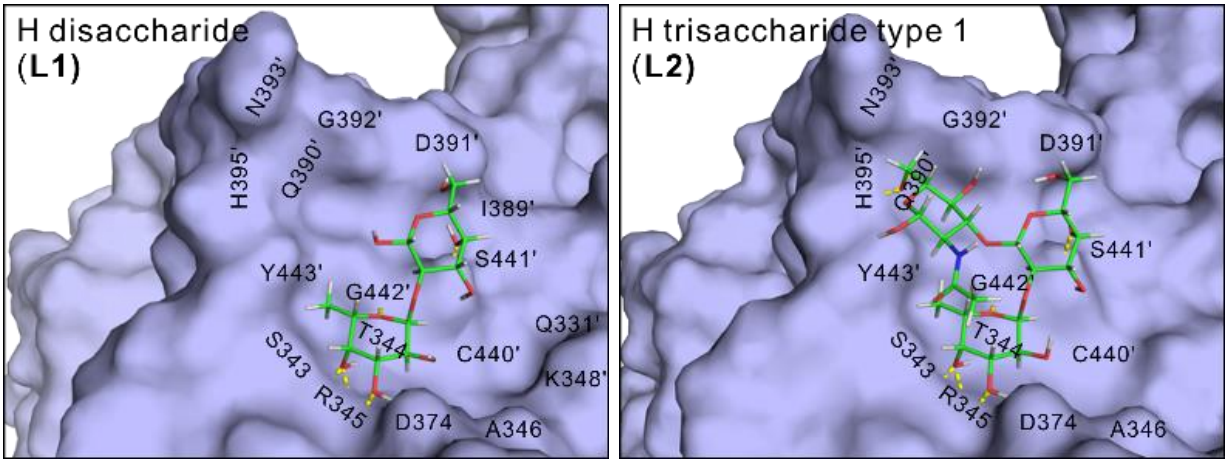

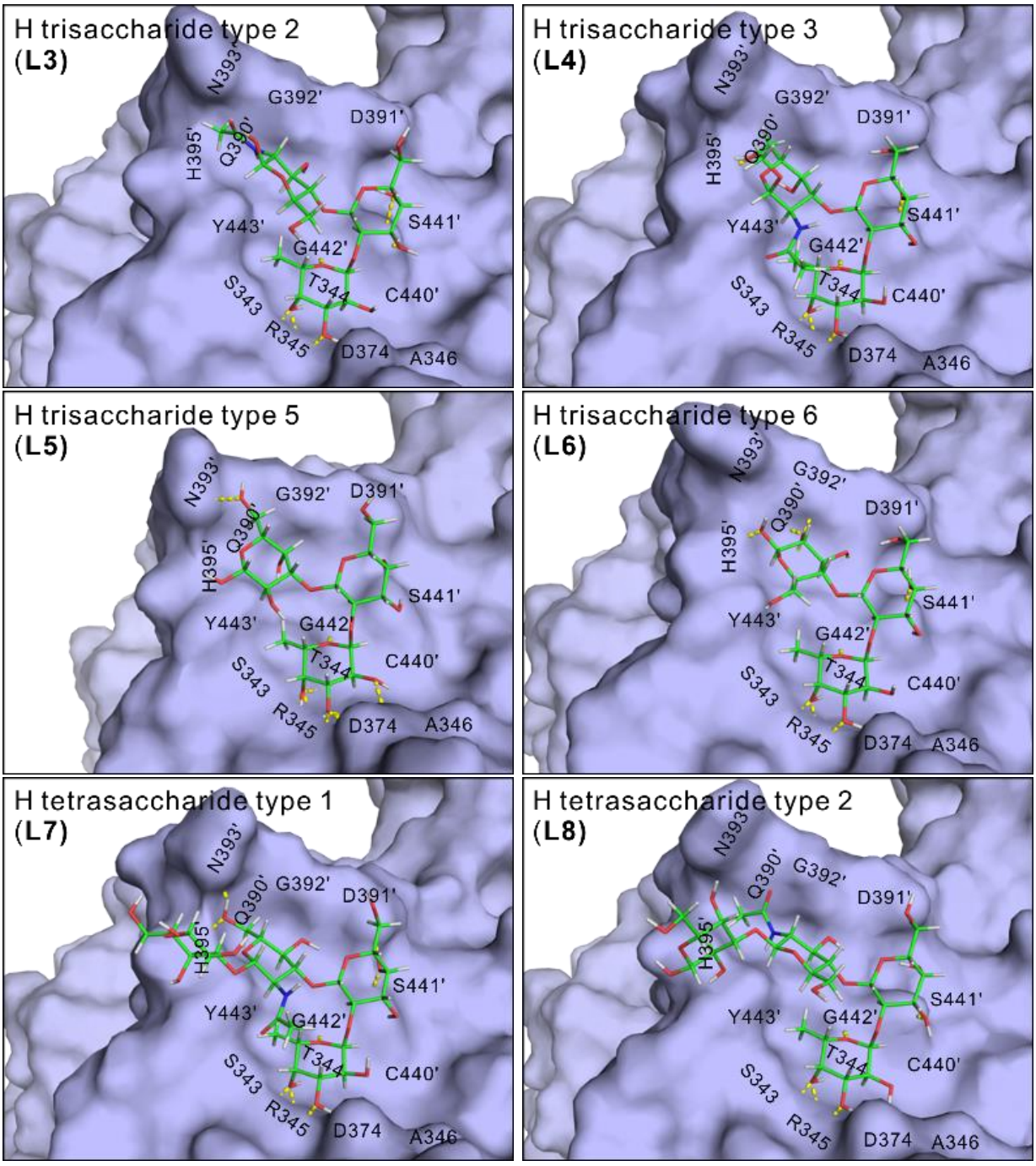
H trisaccharide type 2
(L3)
N393'
G392'
D391'
Q390'
H395'
Y443'
S441'
G442'
T344
C440'
S343
R345
D374
A346
H trisaccharide type 3
(L4)
N393'
G392'
D391'
Q390'
H395'
Y443'
S441'
G442'
T344
C440'
S343
R345
D374
A346
H trisaccharide type 5
(L5)
N393'
G392'
D391'
Q390'
H395'
S441'
Y443'
G442'
T344
C440'
S343
R345
D374
A346
H trisaccharide type 6
(L6)
N393'
G392'
Q390'
D391'
H395'
S441'
Y443'
G442'
T344
C440'
S343
R345
D374
A346
H tetrasaccharide type 1
(L7)
N393'
Q390'
G392'
D391'
H395'
S441'
Y443'
G442'
T344
C440'
S343
R345
D374
A346
H tetrasaccharide type 2
(L8)
N393'
Q390'
G392'
D391'
H395'
S441'
Y443'
G442'
T344
C440'
S343
R345
D374
A346

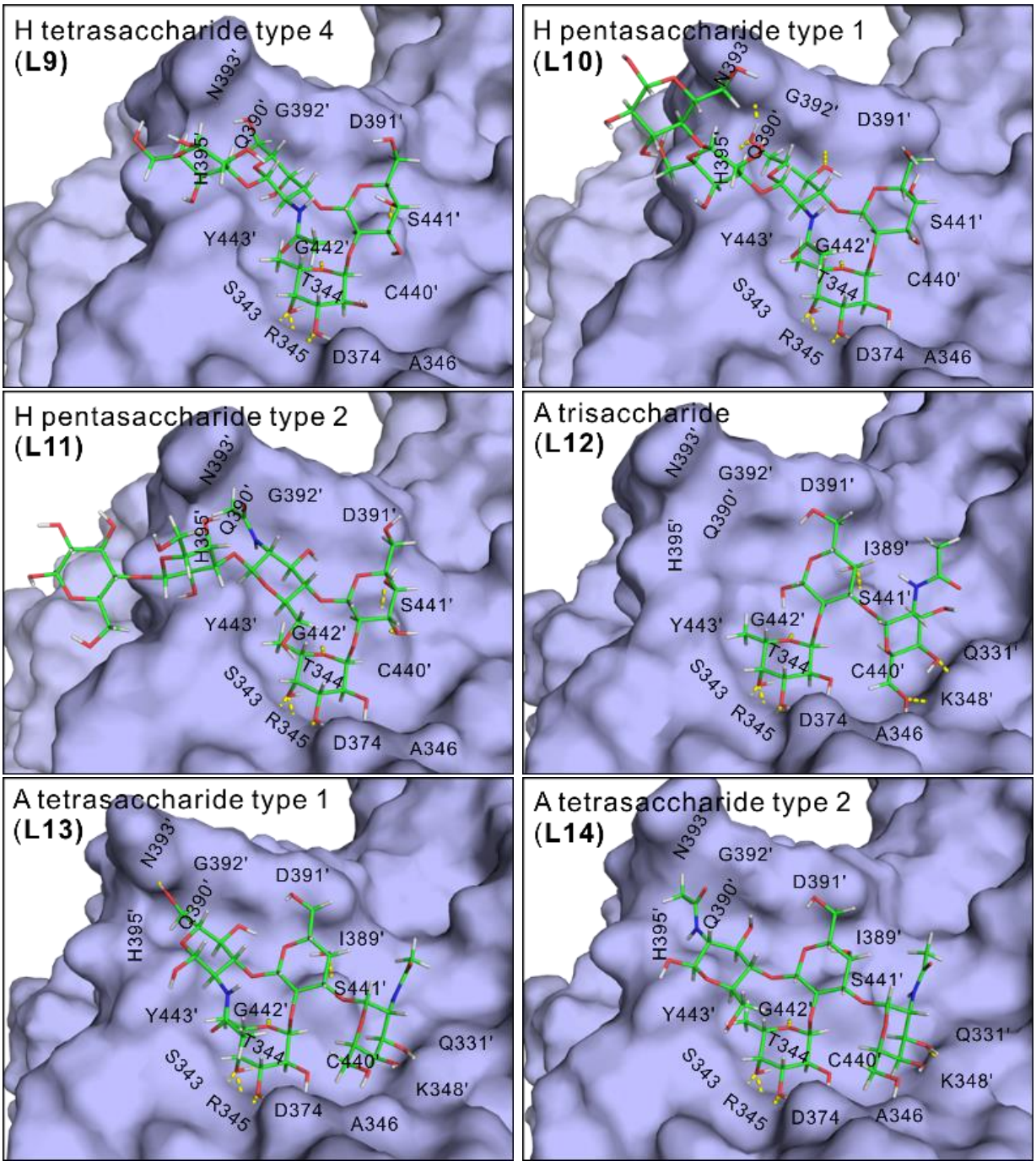
H tetrasaccharide type 4
(L9)
N393'
G392'
D391'
Q390'
H395'
S441'
Y443'
G442'
T344
C440'
S343
R345
D374
A346
H pentasaccharide type 1
(L10)
N393'
G392'
D391'
Q390'
H395'
S441'
Y443'
G442'
T344
C440'
S343
R345
D374
A346
H pentasaccharide type 2
(L11)
N393'
G392'
D391'
Q390'
H395'
S441'
Y443'
G442'
T344
C440'
S343
R345
D374
A346
A trisaccharide
(L12)
N393'
G392'
D391'
Q390'
H395'
I389'
S441'
Y443'
G442'
T344
Q331'
C440'
K348'
S343
R345
D374
A346
A tetrasaccharide type 1
(L13)
N393'
G392'
D391'
Q390'
H395'
I389'
S441'
Y443'
G442'
T344
Q331'
C440'
K348'
S343
R345
D374
A346
A tetrasaccharide type 2
(L14)
N393'
G392'
D391'
Q390'
H395'
I389'
S441'
Y443'
G442'
T344
Q331'
C440'
K348'
S343
R345
D374
A346

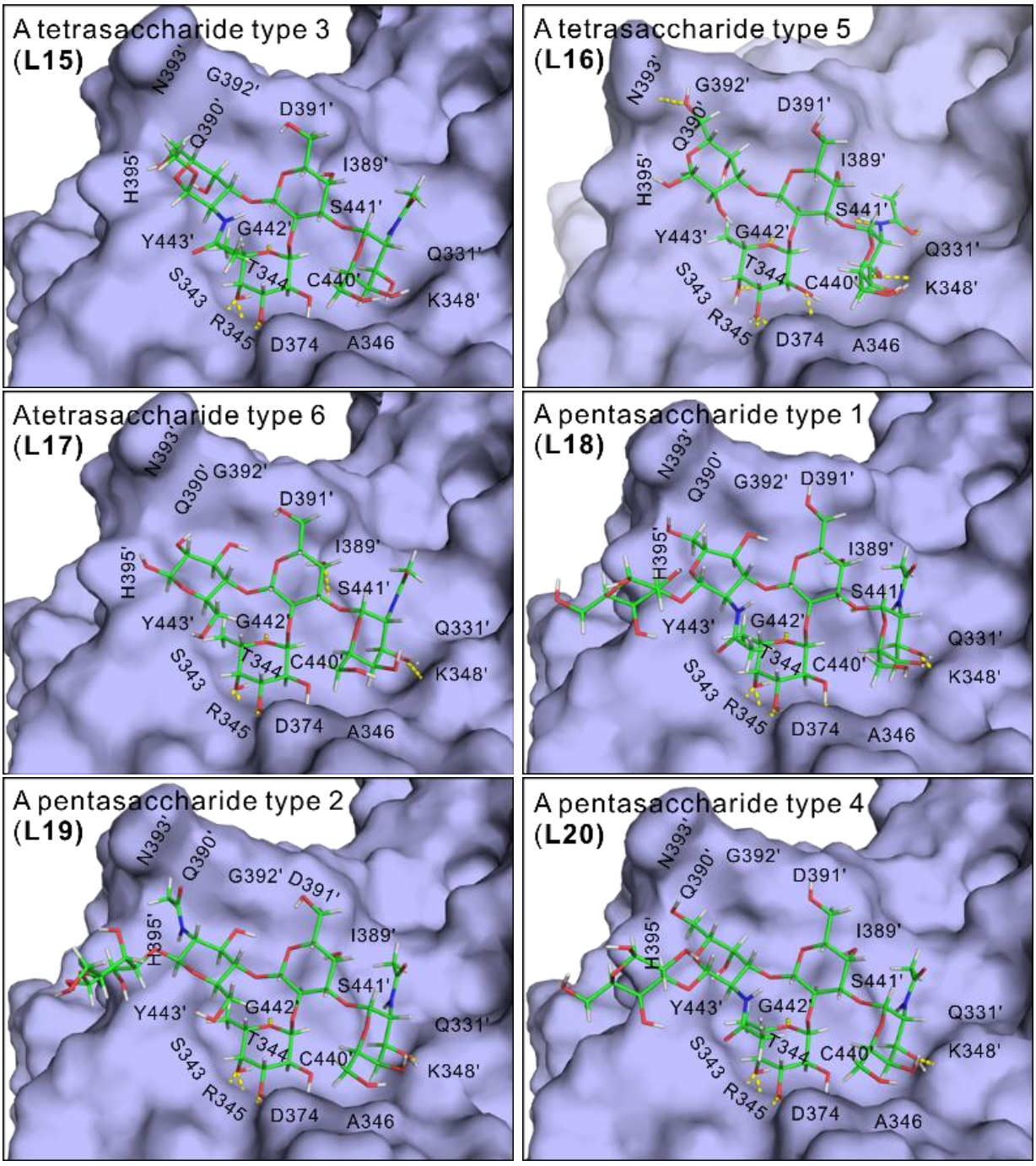
A tetrasaccharide type 3
(L15)
N393'
G392'
Q390'
D391'
I389'
H395'
S441'
Y443'
G442'
Q331'
T344
C440'
K348'
S343
R345
D374
A346
A tetrasaccharide type 5
(L16)
N393'
G392'
Q390'
D391'
I389'
H395'
S441'
Y443'
G442'
Q331'
T344
C440'
K348'
S343
R345
D374
A346
Atetrasaccharide type 6
(L17)
N393'
Q390'
G392'
D391'
I389'
H395'
S441'
Y443'
G442'
Q331'
T344
C440'
K348'
S343
R345
D374
A346
A pentasaccharide type 1
(L18)
N393'
Q390'
G392'
D391'
I389'
H395'
S441'
Y443'
G442'
Q331'
T344
C440'
K348'
S343
R345
D374
A346
A pentasaccharide type 2
(L19)
N393'
Q390'
G392'
D391'
I389'
H395'
S441'
Y443'
G442'
Q331'
T344
C440'
K348'
S343
R345
D374
A346
A pentasaccharide type 4
(L20)
N393'
Q390'
G392'
D391'
I389'
H395'
S441'
Y443'
G442'
Q331'
T344
C440'
K348'
S343
R345
D374
A346

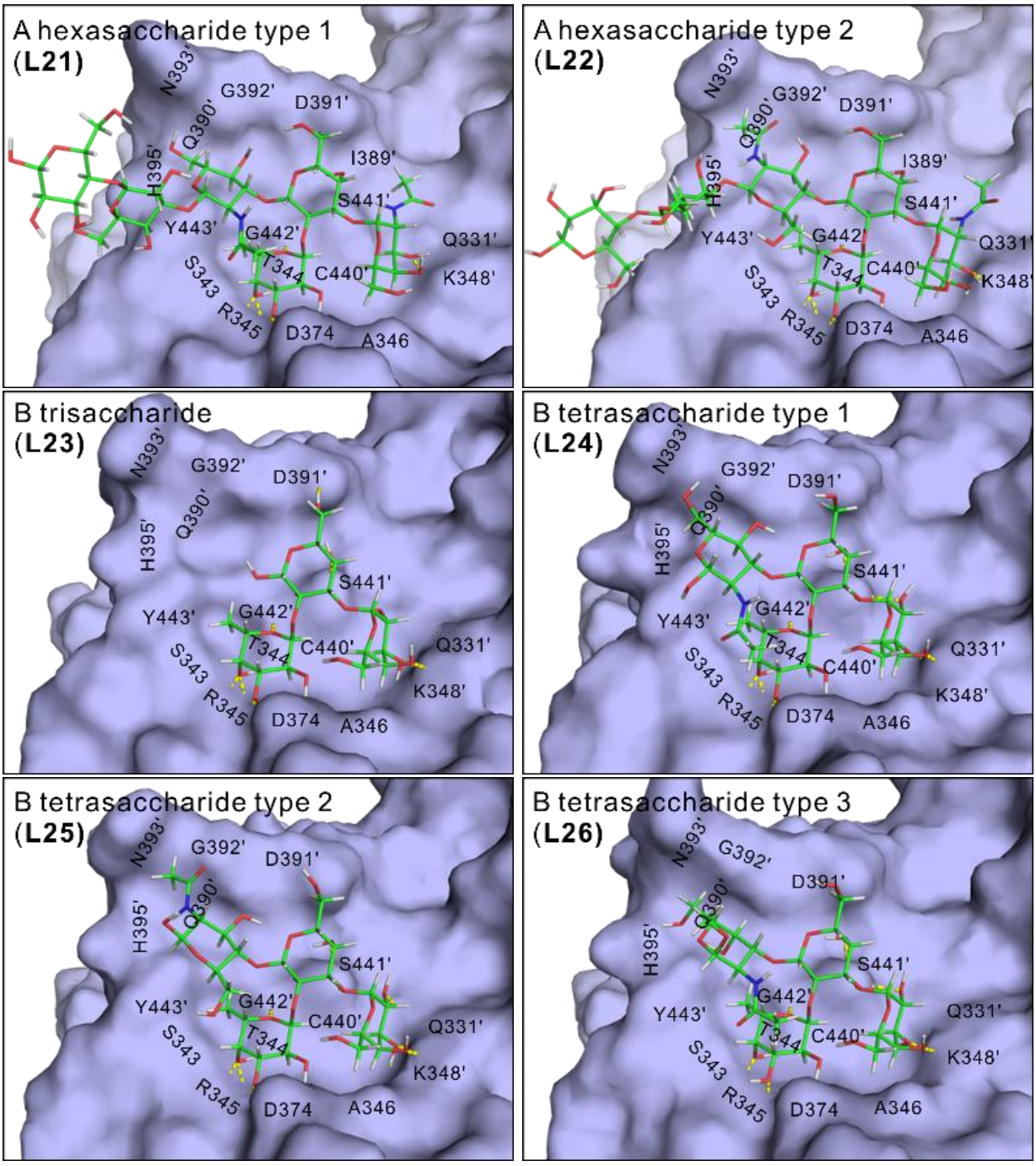
A hexasaccharide type 1
(L21)
N393'
G392'
D391'
Q390'
I389'
H395'
S441'
Y443'
G442'
Q331'
T344
C440'
K348'
S343
R345
D374
A346
A hexasaccharide type 2
(L22)
N393'
G392'
D391'
Q390'
I389'
H395'
S441'
Y443'
G442'
Q331'
T344
C440'
K348'
S343
R345
D374
A346
B trisaccharide
(L23)
N393'
G392'
D391'
Q390'
H395'
S441'
Y443'
G442'
T344
C440'
Q331'
S343
R345
K348'
D374
A346
B tetrasaccharide type 1
(L24)
N393'
G392'
D391'
Q390'
H395'
S441'
Y443'
G442'
T344
C440'
Q331'
S343
R345
K348'
D374
A346
B tetrasaccharide type 2
(L25)
N393'
G392'
D391'
Q390'
H395'
S441'
Y443'
G442'
T344
C440'
Q331'
S343
R345
K348'
D374
A346
B tetrasaccharide type 3
(L26)
N393'
G392'
D391'
Q390'
H395'
S441'
Y443'
G442'
T344
C440'
Q331'
S343
R345
K348'
D374
A346

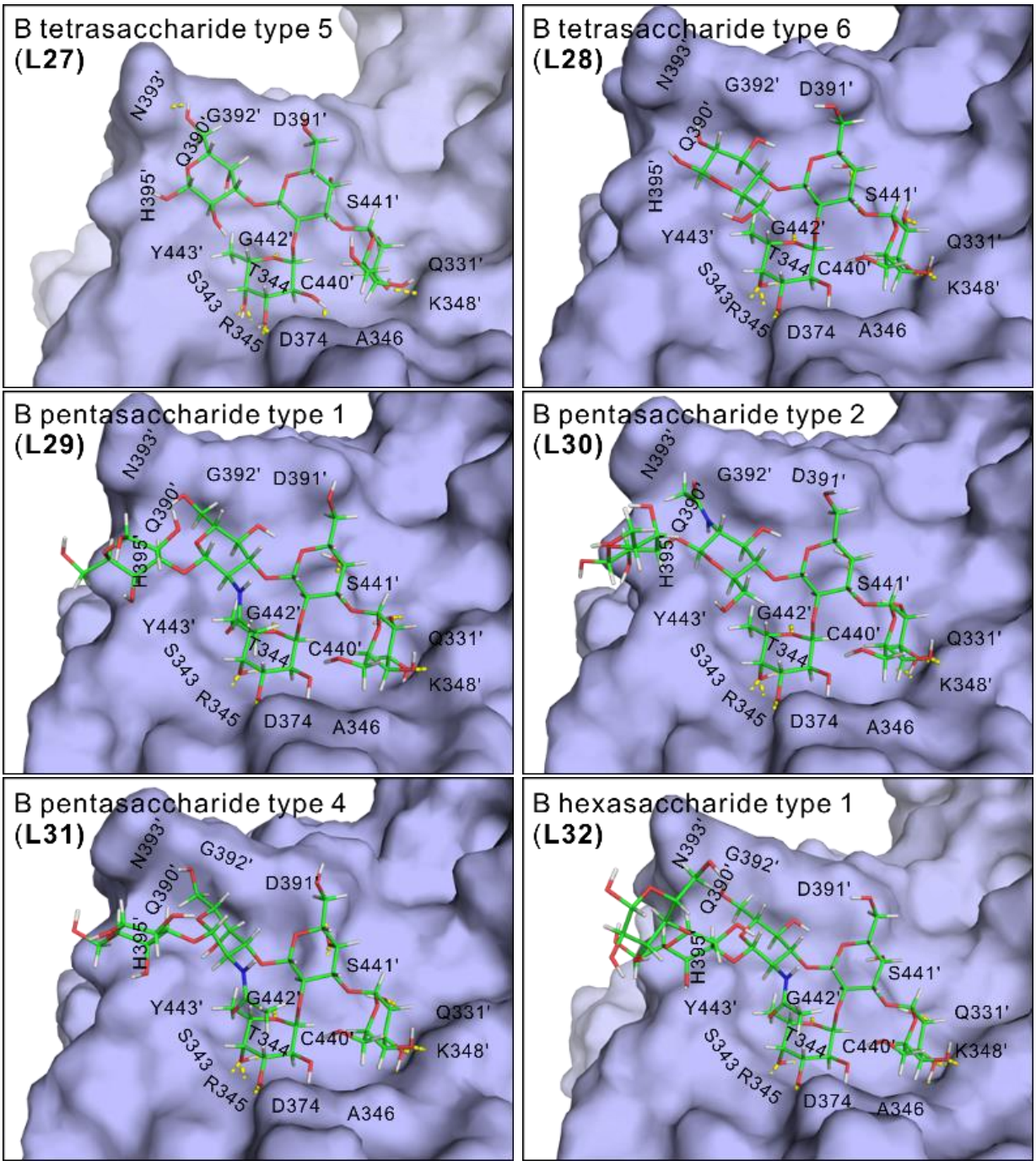
B tetrasaccharide type 5
(L27)
N393'
G392'
D391'
Q390'
H395'
S441'
G442'
Y443'
T344
C440'
Q331'
S343
R345
K348'
D374
A346
B tetrasaccharide type 6
(L28)
N393'
G392'
D391'
Q390'
H395'
S441'
Y443'
G442'
Q331'
T344
C440'
S343R345
K348'
D374
A346
B pentasaccharide type 1
(L29)
N393'
G392'
D391'
Q390'
H395'
S441'
G442'
Y443'
T344
C440'
Q331'
S343
R345
K348'
D374
A346
B pentasaccharide type 2
(L30)
N393'
G392'
D391'
Q390'
H395'
S441'
Y443'
G442'
C440'
Q331'
T344
S343
R345
K348'
D374
A346
B pentasaccharide type 4
(L31)
N393'
G392'
D391'
Q390'
H395'
S441'
Y443'
G442'
Q331'
T344
C440'
S343
R345
K348'
D374
A346
B hexasaccharide type 1
(L32)
N393'
G392'
D391'
Q390'
H395
S441'
Y443'
G442'
Q331'
T344
C440'
S343
R345
K348'
D374
A346

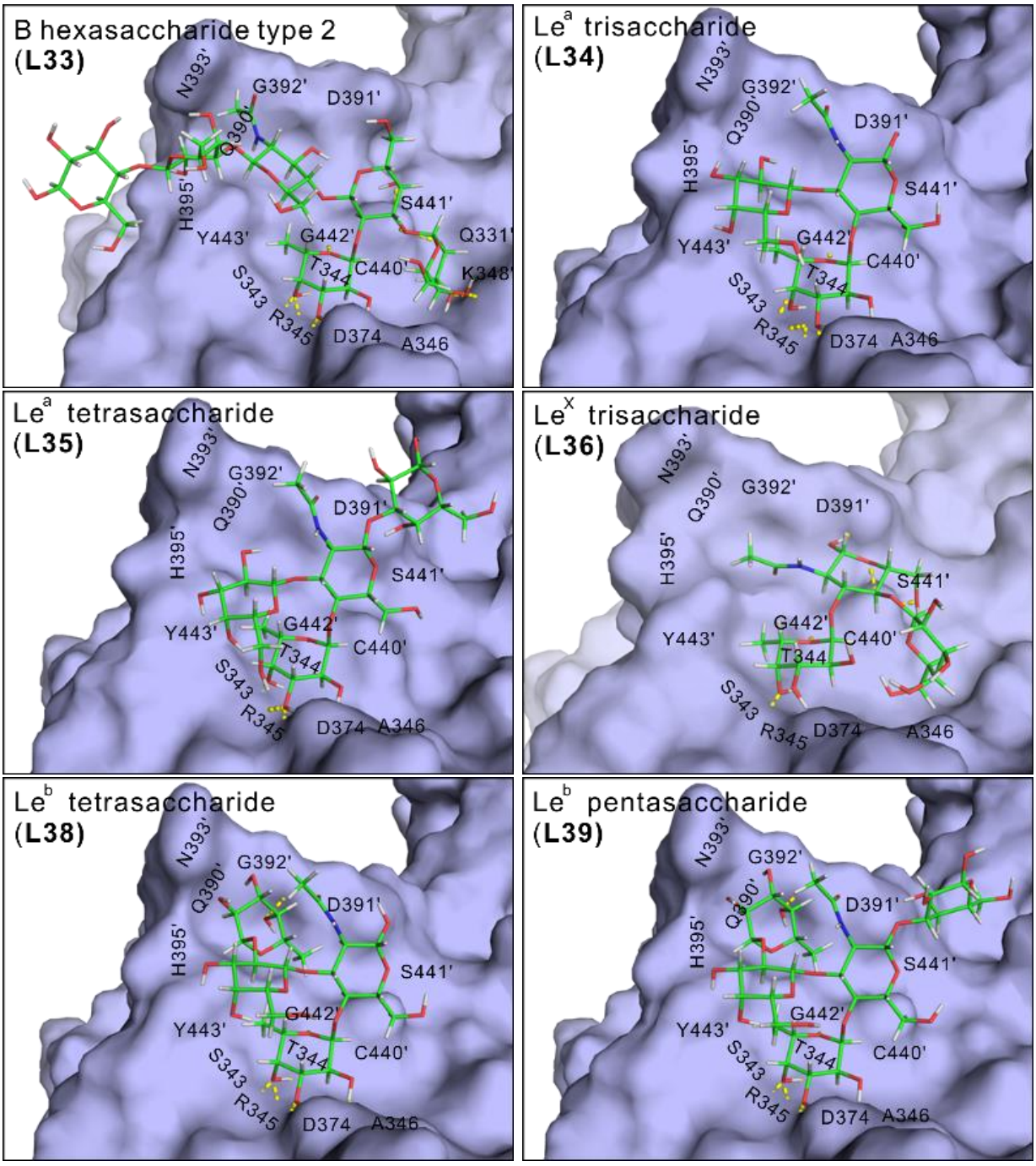
B hexasaccharide type 2
(L33)
N393'
G392'
D391'
Q390'
H395'
S441'
Y443'
G442'
Q331'
T344
C440'
K348'
S343
R345
D374
A346
Le^a trisaccharide
(L34)
N393'
G392'
Q390'
D391'
H395'
S441'
Y443'
G442'
C440'
T344
S343
R345
D374
A346
Le^a tetrasaccharide
(L35)
N393'
G392'
Q390'
D391'
H395'
S441'
Y443'
G442'
C440'
T344
S343
R345
D374
A346
Le^X trisaccharide
(L36)
N393'
Q390'
G392'
D391'
H395'
S441'
Y443'
G442'
C440'
T344
S343
R345
D374
A346
Le^b tetrasaccharide
(L38)
N393'
G392'
Q390'
D391'
H395'
S441'
Y443'
G442'
C440'
T344
S343
R345
D374
A346
Le^b pentasaccharide
(L39)
N393'
G392'
Q390'
D391'
H395'
S441'
Y443'
G442'
C440'
T344
S343
R345
D374
A346

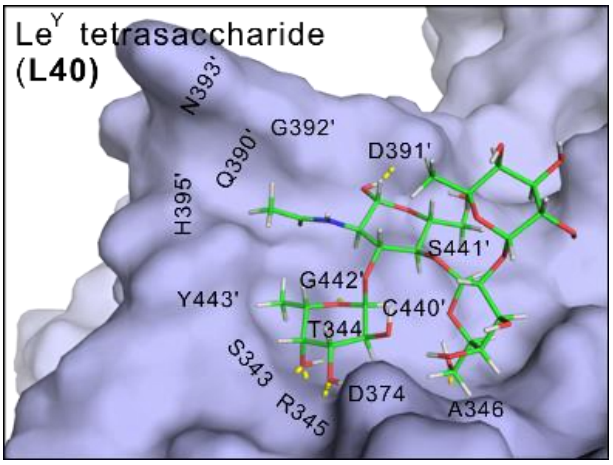
Le^Y tetrasaccharide
(L40)
N393'
G392'
Q390'
D391'
H395'
S441'
G442'
Y443'
C440'
T344
S343
R345
D374
A346